Journal of Advanced Research 63 (2024) 17–33

Contents lists available at ScienceDirect

Journal of Advanced Research

journal homepage: www.elsevier.com/locate/jare

Targeting YTHDF2 inhibits tumorigenesis of diffuse large B-cell lymphoma through ACER2-mediated ceramide catabolism

Xiaomin Chen [a], Tiange Lu [a], Mengfei Ding [a], Yiqing Cai [a], Zhuoya Yu [a], Xiangxiang Zhou [b,d,*], Xin Wang [a,b,c,d,*]

[a] Department of Hematology, Shandong Provincial Hospital, Shandong University, Jinan, Shandong 250021, China
[b] Department of Hematology, Shandong Provincial Hospital Affiliated to Shandong First Medical University, Jinan, Shandong 250021, China
[c] Branch of National Clinical Research Center for Hematologic Diseases, Jinan, Shandong 250021, China
[d] National Clinical Research Center for Hematologic Diseases, the First Affiliated Hospital of Soochow University, Suzhou 251006, China

HIGHLIGHTS

- YTHDF2 served as an oncogene and prognostic predictor in DLBCL.
- YTHDF2 bound to m6A sites of the ACER2 mRNA 3′-UTR to maintain its stability and expression.
- YTHDF2 contributes to endogenous ceramide hydrolysis by regulating ACER2.
- YTHDF2 regulates ACER2 to trigger ceramide catabolism to activate PI3K/AKT and ERK pathways.

GRAPHICAL ABSTRACT

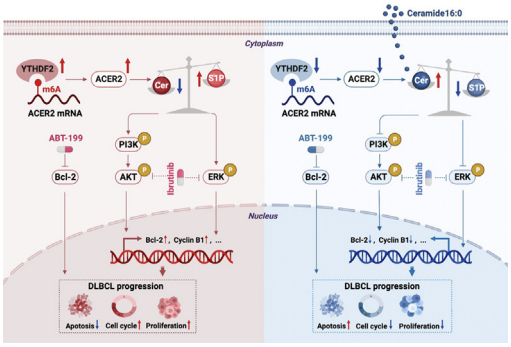

ARTICLE INFO

Article history:
Received 9 July 2023
Revised 17 October 2023
Accepted 18 October 2023
Available online 19 October 2023

Keywords:
DLBCL
YTHDF2
ACER2
Ceramide
Tumorigenesis

ABSTRACT

Introduction: Epigenetic alterations play crucial roles in diffuse large B-cell lymphoma (DLBCL). Disturbances in lipid metabolism contribute to tumor progression. However, studies in epigenetics, especially its critical regulator YTH N6-methyladenosine RNA binding protein 2 (YTHDF2), on lipid metabolism regulation in DLBCL are unidentified.

Objectives: Elucidate the prognostic value and biological functions of YTHDF2 in DLBCL and illuminate the underlying epigenetic regulation mechanism of lipid metabolism by YTHDF2 in DLBCL development.

Methods: The expression and clinical value of YTHDF2 in DLBCL were performed in public databases and clinical specimens. The biological functions of YTHDF2 in DLBCL were determined *in vivo* and *in vitro* through overexpression and CRISPR/Cas9-mediated knockout of YTHDF2. RNA sequencing, lipidomics, methylated RNA immunoprecipitation sequencing, RNA immunoprecipitation-qPCR, luciferase activity assay, and RNA stability experiments were used to explore the potential mechanism by which YTHDF2 contributed to DLBCL progression.

Abbreviations: ACER2, Alkaline ceramidase 2; BTK, Bruton's Tyrosine Kinase; CDS, Coding sequence; DEGs, Differentially expressed genes; DeM, D-*erythro*-MAPP; DMS, N, N-Dimethylsphingosin; DLBCL, Diffuse large B-cell lymphoma; ECOG, Eastern Cooperative oncology Group; ELISA, Enzyme-linked immunosorbent assay; ENI, Extra nodal involvement; ERK, Extracellular regulated protein kinase; GEO, Gene Expression Omnibus; GO, Gene Ontology; H&E, Hematoxylin-eosin; IHC, Immunohistochemistry; IMDM, Iscove's Modified Dulbecco's Medium; IPI, International Prognostic Index; KEGG, Kyoto Encyclopedia of Genes and Genomes; mRNA, Messenger RNA; MeRIP-seq, Methylated RNA immunoprecipitation sequencing; m6A, N6-methyladenosine; NHL, non-Hodgkin's lymphoma; OS, Overall survival; PLS-DA, Partial least squares method-discriminant analysis; PI3K, Phosphatidylinositol 3-kinase; AKT, Protein kinase B; RT-qPCR, Quantitative real-time PCR; RHL, Reactive hyperplasias of lymph nodes; RIP, RNA immunoprecipitation; RNA-seq, RNA sequencing; SCID, Severe combined immunodeficiency; sg, Single-guide; sh, Short hairpin; S1P, Sphingosine-1-phosphate; TCGA, The Cancer Genome Atlas; GETx, The Genotype-Tissue Expression project; UTR, Untranslated region; YTHDF2, YTH N6-methyladenosine RNA binding protein 2.

* Corresponding authors at: Department of Hematology, Shandong Provincial Hospital, Cheeloo College of Medicine, Shandong University, No.324, Jingwu Road, Jinan, Shandong 250021, China (X. Wang) Department of Hematology, Shandong Provincial Hospital, Cheeloo College of Medicine, Shandong University, No.324, Jingwu Road, Jinan, Shandong 250021, China (X. Zhou).

E-mail addresses: xiangxiangzhou@sdu.edu.cn (X. Zhou), xinw007@126.com (X. Wang).

https://doi.org/10.1016/j.jare.2023.10.010

Results: YTHDF2 was highly expressed in DLBCL, and related to poor prognosis. YTHDF2 overexpression exerted a tumor-promoting effect in DLBCL, and knockdown of YTHDF2 restricted DLBCL cell proliferation, arrested cell cycle in the G2/M phase, facilitated apoptosis, and enhanced drug sensitivity to ibrutinib and venetoclax. In addition, YTHDF2 knockout drastically suppressed tumor growth in xenograft DLBCL models. Furthermore, a regulatory role of YTHDF2 in ceramide metabolism was identified in DLBCL cells. Exogenous ceramide effectively inhibited the malignant phenotype of DLBCL cells *in vitro*. The binding of YTHDF2 to m6A sites on alkaline ceramidase 2 (ACER2) mRNA promoted its stability and expression. Enhanced ACER2 expression hydrolyzed ceramides, disrupting the balance between ceramide and sphingosine-1-phosphate (S1P), activating the ERK and PI3K/AKT pathways, and leading to DLBCL tumorigenesis.

Conclusion: This study demonstrated that YTHDF2 contributed to the progression of DLBCL by regulating ACER2-mediated ceramide metabolism in an m6A-dependent manner, providing novel insights into targeted therapies.

Introduction

Diffuse large B-cell lymphoma (DLBCL) is the most common subtype of non-Hodgkin lymphoma (NHL) in adults, exhibiting a pronounced level of aggressiveness and heterogeneity [1]. Approximately two-thirds of individuals diagnosed with DLBCL achieve complete remission with standard first-line therapy [2], while 30–50% of patients exhibit non-responsiveness or experience recurrence [3]. Due to the extensive genetic and epigenetic heterogeneity of DLBCL, the lack of specificity in conventional treatment is even more concerning [4]. Recent studies have demonstrated that epigenetic compounds could reprogram cellular phenotypes, resulting in a novel therapeutic approach that exploits epigenome plasticity to modulate cell response to anti-tumor drugs [5]. Therefore, exploring epigenetic alterations in DLBCL may provide novel insights into the treatment of this disease.

N6-methyladenosine (m6A) methylation, a crucial epigenetic modification, controls a variety of basic bioprocesses [6]. m6A modification is dynamically modulated by methyltransferases, demethylases, and binding proteins, thereby dictating the fate of mRNA by regulating the processes of mRNA stability, transport, translation, and degradation [7–8]. YTH N6-methyladenosine RNA binding protein 2 (YTHDF2), functions as an important m6A-binding protein, and specifically recognizes and binds to m6A sites, resulting in m6A-modified mRNA degradation or translation [9–10]. Growing evidence has shown that YTHDF2 is closely related to tumor growth, proliferation, and survival [11–12]. Our previous studies have revealed that KIAA1429 regulated DLBCL progression through an m6A-YTHDF2-dependent manner [13], indicating the participation of m6A modification in the progression of DLBCL. However, the involvement of YTHDF2 in DLBCL tumorigenesis and the underlying molecular mechanism remain unclear.

Recent studies have demonstrated that aberrant lipid metabolism regulated by a crucial epigenetic modification, m6A methylation, is involved in tumor progression [6,14]. Our previous study has indicated significant associations between aberrant serum lipid metabolism and the survival of lymphoma patients [15]. Lipids are also reported to play a vital role in DLBCL cell proliferation [16]. Sphingolipids, the lipid subclass, are structural molecules of cell membranes with the role of regulating multiple biological processes such as cell proliferation, survival, and apoptosis by mediating various cellular signal transduction [17]. As the common backbone of most sphingolipids, ceramide can be synthesized from membrane sphingomyelin breakdown by sphingomyelinases, and hydrolyzed by ceramidase to produce sphingosine [18]. In turn, phosphorylation of sphingosine by sphingosine kinase (SphK) could generate sphingosine 1 phosphate (S1P) [19]. Ceramide has been demonstrated to inhibit proliferation and cause apoptosis, while S1P has been positively linked to survival in cells [20]. The balance between S1P and ceramide, known as the S1P/ceramide axis, is recognized as a crucial signaling initiator to regulate cell survival, death, and proliferation [21]. The expression levels of ceramide synthesis and metabolism genes, which are critical for maintaining ceramide levels and subsequent production of S1P levels, are regulated by several factors, including transcription factors, epigenetic modifications, and signaling pathways [22]. Alkaline ceramidase 2 (ACER2/ASAH3L) has been demonstrated to control both intracellular and extracellular sphingomyelin production by hydrolyzing ceramide [23]. At present, efforts to rescue the apoptotic phenotype by restoring ceramide accumulation or restricting S1P signaling have received extensive attention [24–25]. However, the contact between epigenetic regulation, especially its crucial regulator YTHDF2, and the S1P/ceramide axis in the development of DLBCL remains unclear.

This study focused on the biological functions of YTHDF2 in DLBCL and interrogated the molecular mechanism by which YTHDF2 is involved in the development of DLBCL through epigenetic regulation of ceramide metabolism and S1P/ceramide axis. These findings might provide citations for forthcoming drug advancements and treatment strategies.

Material & methods

Clinical samples

A total of 104 *de novo* DLBCL patients and 20 patients with reactive hyperplasias of lymph nodes (RHL) were enrolled in this study with informed consent, and the lymph node samples were collected. Isolation of peripheral blood mononuclear cells (PBMCs) from three healthy samples was conducted. Normal B cells were purified from the isolated PBMCs with a $CD19^+$ magnetic microbeads kit (Miltenyi Biotec, Bergisch Gladbach, Germany). All samples were collected with informed consent and approved by the Medical Ethical Committee of Shandong Provincial Hospital.

Cell lines and reagents

Cultures of human DLBCL cell lines OCI-LY1, OCI-LY3, OCI-LY8, and U2932 were conducted at 37 °C with 5% CO_2 in Iscove's Modified Dulbecco's Medium (IMDM) (Gibco, CA, USA) containing 10% fetal bovine serum (HyClone, UT, USA) and 1% penicillin–streptomycin as described previously [26]. Ceramide 16:0, a sphingolipid, was purchased from Avanti (AL, USA). D-*erythro*-MAPP (DeM), an inhibitor of ceramidases, and N, N-Dimethylsphingosine (DMS), a specific inhibitor of SphK were acquired from MedChemExpress

(NJ, USA). Ibrutinib and venetoclax were obtained from Selleck (TX, USA).

Establishment of stable knockdown and overexpression of YTHDF2 cell lines

Lentivirus vectors encoding either short hairpin (sh) YTHDF2, YTHDF2 overexpression, or their empty lentiviral vector (control) were established from GeneChem (Shanghai, China). The RNAi sequences are shown in **Supplementary Table S2**. According to the instructions of the manufacturer, lentivirus transfection was executed in OCI-LY1 and OCI-LY3 cell lines [27]. The selection of stably transfected cells was performed with 5 μg/ml puromycin (AMRESCO, HY-B1743S) 72 h (h) later.

CRISPR/Cas9-mediated accomplishment of YTHDF2-knockout cells

The CRISPR/Cas9 genomic editing system was employed to create YTHDF2 knockout OCI-LY1 cells, utilizing three distinct single-guide RNAs (sgRNAs) that targeted the deletion of YTHDF2 (sgYTHDF2). A non-targeting sgRNA (sgCon) was the control. Lentiviral vectors with stably expressing Cas9-gRNA were obtained from OBiO (Shanghai, China) as described before [28]. The constructed vector was pLenti-U6-spgRNA (YTHDF2)-CMV-Puro-P2A-3Flag-spCas9. Stably transfected cells were filtered by 5 μg/ml puromycin (HY-B1743S, AMRESCO) after 72 h, and then monoclonal cells were selected through limiting dilution and continued to expand.

Knockdown of ACER2 in DLBCL cells

The establishment of ACER2 knockdown plasmids using the vector pLent-U6-GFP-Puro was performed by Boshang Biotechnology (Jinan, China). With Lipofectamine 2000 (Invitrogen, 11668019), the ACER2 shRNA plasmids and an empty vector were transfected with OCI-LY1 and OCI-LY3 cells, YTHDF2-deficient cells, and the corresponding control cells, following the manufacturer's instructions [27]. The sequences are shown in **Supplementary Table S2**.

Cell proliferation assay

Assaying cell proliferation was performed by the Cell Counting Kit-8 (CCK-8) assay (Dojindo, Kumamoto, Japan), as described previously [29]. 1×10^4 pretreated DLBCL cells were seeded in 96-well plates for 24-72 h, and then incubated with 10 μl of CCK-8 per well for 3 h at 37 °C. Absorbance at 450 nm was measured through a Multiskan GO Microplate Reader (Thermo Scientific, USA).

Flow cytometric analysis

Both cell cycle and apoptosis were detected by flow cytometry (Navios, Beckman Coulter, CA, USA). For cell cycle analysis, after collection and washing twice with PBS, the DLBCL cells were fixed with 70% ethanol at -20 °C overnight, followed by resuspending in PI/RNase staining solution (BD Biosciences, MA, USA). ModFit LT version 3.2 calculated the proportion of cells in distinct cell cycle phases. Cell apoptosis was analyzed using Annexin V-PE/7AAD assay staining (BD Biosciences), following the manufacturer's instructions [30].

m6A methylation assay

According to the manufacturer's instructions [13], the m6A RNA methylation quantification kit (Epigentek, NY, USA) was used to measure the m6A content in 200 ng of total RNA from DLBCL cells. A standard curve was prepared with a concentration from 0.01 to 0.5 ng/μl. The 96-well plate was paved evenly with RNA samples. Subsequently, the diluted capture antibody, diluted detection antibody, and diluted enhancer solution were introduced into each well. The absorbance at 450 nm was measured with a microplate reader to determine the m6A levels. The amount of m6A was computed as m6A (ng) = (sample OD – NC OD)/slope.

Enzyme-linked immunosorbent assay (ELISA)

Ceramide and S1P levels in cell extracts were determined by ELISA kits (mlbio, Shanghai, China), respectively. Cellular ceramide or S1P was captured by solid-phase antibody and then combined with horseradish peroxidase (HRP)-labeled detection antibody to form an antibody-antigen-enzyme-antibody complex as described previously [31]. For color development, the substrate TMB was added after thorough washing. A standard curve was generated by measuring the absorbance at 450 nm through a Multiskan GO Microplate Reader (Thermo Scientific, USA) to calculate the amount of ceramide or S1P in the samples.

Dual-luciferase reporter assay

An amplification of 3′-UTR of ACER2 containing the binding site of YTHDF2 and mutant sequences were cloned respectively into the GV272 vector (GeneChem). Cells were plated in 96-well plates and co-transfected with GV272-ACER2 3′-UTR-WT or GV272-ACER2 3′-UTR-MUT and Renilla luciferase plasmids. Renilla luciferase was normalized to firefly luciferase activity after collecting the cells at 48 h. Dual-Luciferase Reporter Assay Systems (Promega, Madison, US) was used for Luciferase reporter assays as described before [32].

Bioinformatic analysis

The gene expression profiles and clinicopathological information were obtained from The Cancer Genome Atlas (TCGA) database, the Genotype-Tissue Expression project (GETx), and the Gene Expression Omnibus (GEO, GSE117556, and GSE32918). Differential expression analysis was executed using the "Limma" package as described before [33]. Kaplan-Meier method was used to generate overall survival (OS) curves. Univariate and multivariate Cox regression analyses were utilized to verify whether YTHDF2 and relevant clinicopathologic characteristics were independent prognostic parameters for DLBCL patients. Visualization of Gene Ontology (GO) terms and Kyoto Encyclopedia of Genes and Genomes (KEGG) pathways were conducted by the "ggplot2" R package.

Hematoxylin-eosin (H&E) and immunohistochemistry (IHC) staining

The tumors were immobilized in a 4% paraformaldehyde solution, subsequently encased in paraffin, sliced into sections, and subjected to staining with hematoxylin and eosin (H&E) and IHC, as described in the previous study [13]. IHC was conducted on slides from tumor tissues of DLBCL patients and mice. After dewaxing and rehydration, tissue sections were treated with the EDTA antigen retrieval solution (pH 8.0). Then, 3% H_2O_2 was used to intercept endogenous peroxidase, and normal goat serum blocked nonspecific binding. Incubation with primary antibodies anti-YTHDF2 (24744–1-AP, Proteintech, Wuhan, China) or anti-Ki67 (27309–1-AP, Proteintech) was performed on tissue slides. A secondary antibody conjugated to HRP (SP9001, Zhongshan Goldenbridge, Beijing, China) was then applied to tissue sections, and a 3,3-diaminobenzidine (DAB) Kit (Zhongshan Goldenbridge) was used for IHC staining. Hematoxylin counterstained sections were

evaluated with ImageJ software. Two researchers respectively scored the immunoreactivity intensity as 3 (strong), 2 (medium), 1 (weak), and 0 (no staining), and the percentage of positively stained cells was scored as 0 (<5%), 1 (5–25%), 2 (25–50%), 3 (50–75%), and 4 (more than 75%).

Western blotting

Cell lysates were extracted using RIPA buffer (Pierce) together with inhibitors for proteases and phosphatases (PhosSTOP, Roche, Basel, Switzerland). Protein abundance was analyzed by SDS-PAGE and then transferred onto polyvinylidene fluoride membranes to perform immunoblotting. Following the previous description, western blotting analysis was conducted [26]. The primary antibodies used were as follows: anti-YTHDF2 (24744–1-AP, Proteintech), anti-ACER2 (ABP57426, Abbkine), anti-caspase3 (14220, Cell Signaling Technology (CST)), anti-Cleaved-caspase3 (9664, CST), anti-caspase9 (9508, CST), anti-Cleaved-caspase9 (92873, CST), anti-Bcl-2 (ab32124, Abcam), anti-p21 (2947, CST), anti-Cyclin B1 (4138, CST), anti-GAPDH (TA-08, Zhongshan Goldenbridge), anti-β-tubulin (86298, CST), and anti-β-actin (TA-09, Zhongshan Goldenbridge). Following overnight incubation with primary antibodies at 4 °C, membranes were washed with TBS-T and then treated with HRP-conjugated secondary antibody (Zhongshan Goldenbridge). Images were captured with the Amersham Imager 600 imaging system (General Electric, USA).

Quantitative real-time PCR (RT-qPCR)

According to the manufacturer's instructions [34], total RNA was isolated by Trizol reagent (TaKaRa, Shiga, Japan), and the cDNA library was constructed by an Evo M-MLV RT Kit (AG11706, Accurate Biology, China). RT-qPCR amplification reaction was performed on a LightCycler 480II system (Roche) using SYBR Green Premix Pro Taq HS qPCR Kit (AG11701, Accurate Biology). The primers are shown in **Supplementary Table S1**. The △△CT method was used to calculate relative quantification.

RNA immunoprecipitation (RIP) assay

RIP analysis was conducted utilizing an RNA Immunoprecipitation Kit (BersinBio, Guangzhou, China), as described before [13]. In brief, DNA was removed after cell lysis, 1.7 ml of lysate was obtained, including 0.1 ml as input, and the remainder was divided into two parts. Equilibrated magnetic Protein A/G beads coated with 4 μg of anti-YTHDF2 (24744–1-AP, Proteintech) or IgG control antibodies were incubated at 4 °C overnight with the indicated cell lysates. An ND-1000 was used to analyze the purity and concentration of immune-precipitated RNA after purification with phenol: chloroform: isoamyl alcohol (25:24:1). Gene enrichment was calculated from qPCR detection of YTHDF2-bound RNA, normalized to input.

RNA stability assay

OCI-LY1 cells with or without YTHDF2 deletion were exposed to actinomycin D (A9415, Sigma), a transcriptional inhibitor, at a concentration of 5 μg/ml to suppress mRNA transcription [13]. Cells were harvested after 0, 50, 100, and 150 mins of incubation, and then total RNA was isolated for qPCR.

RNA sequencing (RNA-seq)

Extraction of total RNA from 3 stable YTHDF2 knockout OCI-LY1 cells and their relevant non-target controls was performed using RNAiso Plus (TaKaRa), followed by the construction of a sequencing library [28]. 150-bp paired-end reads were generated using an Illumina NovaSeq platform for sequencing the library preparations (Novogene, China). Paired-end clean reads were aligned to the reference genome index built using Hisat2 v2.0.5. With the "DESeq2" R package, differential expression analysis was conducted.

Methylated RNA immunoprecipitation sequencing (MeRIP-seq)

MeRIP and library preparation were performed at Novogene as described before [13]. In brief, 300 μg of RNAs were separately collected from the OCI-LY1 cells with or without YTHDF2 deletion. Sequencing was performed using three independent biological replicates. The Agilent 2100 bioanalyzer (Agilent) and the simpliNano spectrophotometer (GE Healthcare) were employed for the evaluation of RNA integrity and concentration. In immunoprecipitation experiments, fragmented mRNA (∼100 nt) was incubated with an anti-m6A polyclonal antibody (Synaptic Systems). The immunoprecipitated mRNA or input was utilized for the construction of the library, which was prepared using the NEBNext Ultra RNA Library Prepare Kit for Illumina (New England Biolabs).

Lipidomics analysis

OCI-LY1 cells with or without YTHDF2 knockout were collected, and 800 μl of precooling buffer solution dichloromethane/methanol (3:1) was used to extract lipids. Lipidomics analysis was performed by BGI (Shenzhen, China) as described before [35]. The SPLASHTM Lipidomix Mass Spec Standard (Avanti Polar Lipids, USA) was used as an internal standard. Lipids were separated and detected by an LC-MS system consisting of Waters 2D UPLC (Waters, USA) and Q Exactive high-resolution mass spectrometer (Thermo Fisher Scientific, USA). The screening criteria for differential lipid molecules were as follows: fold change ≥ 1.2 or ≤ 0.83, p-value < 0.05.

In vivo subcutaneous xenograft model

All animal experiments were conducted according to the guidelines set forth by the Animal Care and Research Advisory Committee of Shandong Provincial Hospital. Female severe combined immunodeficiency (SCID) beige mice (n = 28) aged 5 weeks were purchased from Beijing Vital River Laboratory Animal Technology Co., Ltd. (Beijing, China) and bred in pathogen-free conditions (n = 7 per group). 1×10^7 YTHDF2 stable knockout OCI-LY1 cells or YTHDF2 overexpression OCI-LY1 cells mixed with 100 μl Matrigel (356234, BD Biosciences) were injected subcutaneously into the right armpit of mice. The tumor size was measured with a digital caliper every other day, and tumor volume was calculated as $V = (a \times b^2)/2$, among which a is the largest dimension and b is the vertical diameter. Mice were culled once the tumor volume reached 2000 mm^3, and all remaining mice were sacrificed after 4 weeks.

Ethics statement

All samples were collected from patients with informed consent and approved by the Medical Ethical Committee of Shandong Provincial Hospital (Approval no.2021–217, date: 1 March 2021). All experiments involving animals were conducted according to the ethical policies and procedures approved by Animal Care and Research Advisory Committee of Shandong Provincial Hospital (Approval no.2021–217, date: 1 March 2021).

Statistical analysis

Log-rank test was used to compare differences between the groups based on OS estimates generated by Kaplan-Meier. Univariate and multivariate Cox regression analyses were used to verify whether YTHDF2 and relevant clinicopathologic characteristics were independent prognostic parameters for DLBCL patients. Correlation analysis was subjected to a Pearson correlation test. A minimum of three replicates were conducted in all experimental trial, and the results were reported as mean ± standard deviation (SD). The statistical methods employed were Student's t-tests and one-way analysis of variance (ANOVA) were applied to evaluate the disparities between groups. A statistically significant difference was defined as $p < 0.05$. Statistical analyses were performed utilizing R version 3.6.0, SPSS Statistics version 20.0, and GraphPad Prism 8.0.

Results

YTHDF2 was upregulated in DLBCL and correlated with poor prognosis

The data from the GEO database (GSE32018) was first investigated the expression patterns of YTHDF2. Compared to normal samples, expression of YTHDF2 was significantly higher in DLBCL patients (Fig. 1A). Similarly, YTHDF2 displayed a higher expression in DLBCL through integrating data of 337 whole blood samples from the GETx database and 48 DLBCL samples from TCGA database (Fig. 1B). In addition, the univariate analysis indicated that YTHDF2 ($p = 0.007$, HR = 2.182), age ($p = 0.015$, HR = 1.031), stage ($p = 0.004$, HR = 1.559), Eastern Cooperative oncology Group (ECOG) score ($p = 0.001$, HR = 1.654), lactate dehydrogenase (LDH) ($p < 0.001$, HR = 1.001), and International Prognostic Index (IPI) score ($p < 0.001$, HR = 1.810) were remarkably associated with OS (Fig. 1C). Combining all these parameters into multivariate Cox regression analysis, YTHDF2 ($p = 0.049$, HR = 1.812), LDH ($p = 0.007$, HR = 1.000), and IPI score ($p = 0.003$, HR = 1.672) were still identified as independent poor prognostic factors for OS of DLBCL patients (Fig. 1D).

Consistent with the observation above, YTHDF2 expression was increased in DLBCL cell lines, both at the mRNA and protein levels, compared to normal $CD19^+$ B cells (Fig. 1E-F). Furthermore, the expression of YTHDF2 was shown to be higher in DLBCL tissues compared to RHL tissues, as determined by IHC staining (Fig. 1G). Based on the cut-off value determined from ROC curve, the positive rate of YTHDF2 in DLBCL tissues was identified as 83% (86of104) and 10% (2of20) in RHL tissues, respectively (**Supplementary** Fig. S1A-B). The relevance between YTHDF2 expression and clinicopathological parameters of DLBCL patients with complete prognostic information was subsequently evaluated. Elevated levels of YTHDF2 expression were found to be correlated with advanced Ann Arbor stage ($p < 0.0001$) and high IPI score ($p = 0.007$) in DLBCL patients (Table 1). Additionally, the survival analysis revealed a significant correlation between positive YTHDF2 expression and poorer OS in DLBCL patients ($p = 0.013$, Fig. 1H). Collectively, these findings provide evidence that YTHDF2 exerts a significant influence on the prognosis of DLBCL.

Knockdown of YTHDF2 reduced cell proliferation, cell cycle arrest, and increased apoptosis in DLBCL

The potential function of YTHDF2 in DLBCL was investigated through functional enrichment analysis of the gene profiles containing YTHDF2 and its related genes. GO analysis revealed that YTHDF2 appeared to be closely related to cell cycle checkpoint and intrinsic apoptotic signaling pathway (**Supplementary** Fig. S2A). KEGG analysis found YTHDF2 to be enriched in pathways associated with cancer progression including the chemokine signaling pathway and NOD-like receptor signaling pathway (Supplementary Fig. S2B). Subsequently, YTHDF2 knockdown models in both OCI-LY1 and OCI-LY3 cells were established, and shYTHDF2#3 was validated to be remarkably silenced at the protein level in both OCI-LY1 and OCI-LY3 cells (Fig. 2A). As measured by CCK-8, knockdown of YTHDF2 significantly inhibited the cell proliferation of DLBCL cells (Fig. 2B). Moreover, YTHDF2 knockdown increased the G2/M phase ratios in DLBCL cells (Fig. 2C). Decreased expression of Cyclin B1, a marker of G2/M phase, and increased p21 expression, a cell-cycle inhibitor, were observed in cells with YTHDF2 knockdown (Supplementary Fig. S2C). Similarly, in contrast to the control group, deletion of YTHDF2 facilitated cell apoptosis in DLBCL (Fig. 2D). Knockdown of YTHDF2 in DLBCL cells displayed reduced expression of anti-apoptotic protein B-cell lymphoma-2 (Bcl-2) and enhanced the expression of pro-apoptotic markers, including Cleaved-caspase3 and Cleaved-caspase9, indicating the pro-apoptotic feature of YTHDF2 inhibition (**Supplementary** Fig. S2D). These findings indicated that suppression of YTHDF2 inhibited DLBCL cell survival by repressing cell proliferation, arresting the cell cycle, and facilitating apoptosis.

CRISPR/Cas9-targeted knockout of YTHDF2 inhibited cell growth both in vitro and in vivo

The knockout of YTHDF2 in OCI-LY1 cells using a CRISPR/Cas9 genome editing system was constructed to address the mechanism of YTHDF2. Deletion of YTHDF2 in monoclonal cells was substantiated at protein levels (Supplementary Fig. S2E). The deletion of YTHDF2 in DLBCL led to the inhibition of cellular proliferative capacity (Supplementary Fig. S2F) and accumulation in the G2/M phase of the cell cycle (Supplementary Fig. S2G). A low level of Cyclin B1 and a high level of p21 were observed in DLBCL cells with YTHDF2 knockout (Supplementary Fig. S2H). Concurrently, YTHDF2 knockout resulted in a higher rate of apoptosis in DLBCL cells compared to the control group (Supplementary Fig. S2I). Meanwhile, a dramatic decrease of Bcl-2 and elevated cleaved structures of caspase3 and caspase9 were detected in YTHDF2 knockout cells (Supplementary Fig. S2J).

Furthermore, subcutaneous injection of YTHDF2 knockout cells was performed on SCID beige mice to explore its biological function *in vivo* (n = 6 per group) (Fig. 2E). Compared to the control group, tumors with YTHDF2 depletion demonstrated a significant decrease in growth rate and tumor volume (Fig. 2**F-G**), with reduced expression of cell proliferation-related protein Ki67 (**Supplementary** Fig. S2K). Collectively, these data suggested that knockout of YTHDF2 suppressed DLBCL progression both *in vitro* and *in vivo*.

YTHDF2 overexpression exerted tumor-promoting effects in DLBCL

OCI-LY1 and OCI-LY3 cells were transfected with YTHDF2 overexpression lentivirus to further validate the biological function of YTHDF2 in DLBCL. Overexpression of YTHDF2 protein was confirmed in DLBCL cells (Fig. 2H). YTHDF2 overexpression significantly enhanced cell proliferation (Fig. 2I) and decreased the proportion of cells in the G2/M phase (Fig. 2J). Moreover, increased Cyclin B1 expression and decreased p21 expression were shown in DLBCL cells with YTHDF2 overexpression (Fig. 2K). Overexpression of YTHDF2 also inhibited apoptosis of DLBCL cells through Annexin V-PE/7AAD apoptotic assays (Fig. 2L). Besides, expression of Bcl-2 was elevated and the cleaved forms of caspase3 and caspase9 were notably declined in YTHDF2-overexpressing cells (Fig. 2M).

Additionally, xenograft DLBCL models were constructed with YTHDF2-overexpressing cells in SCID beige mice to evaluate the

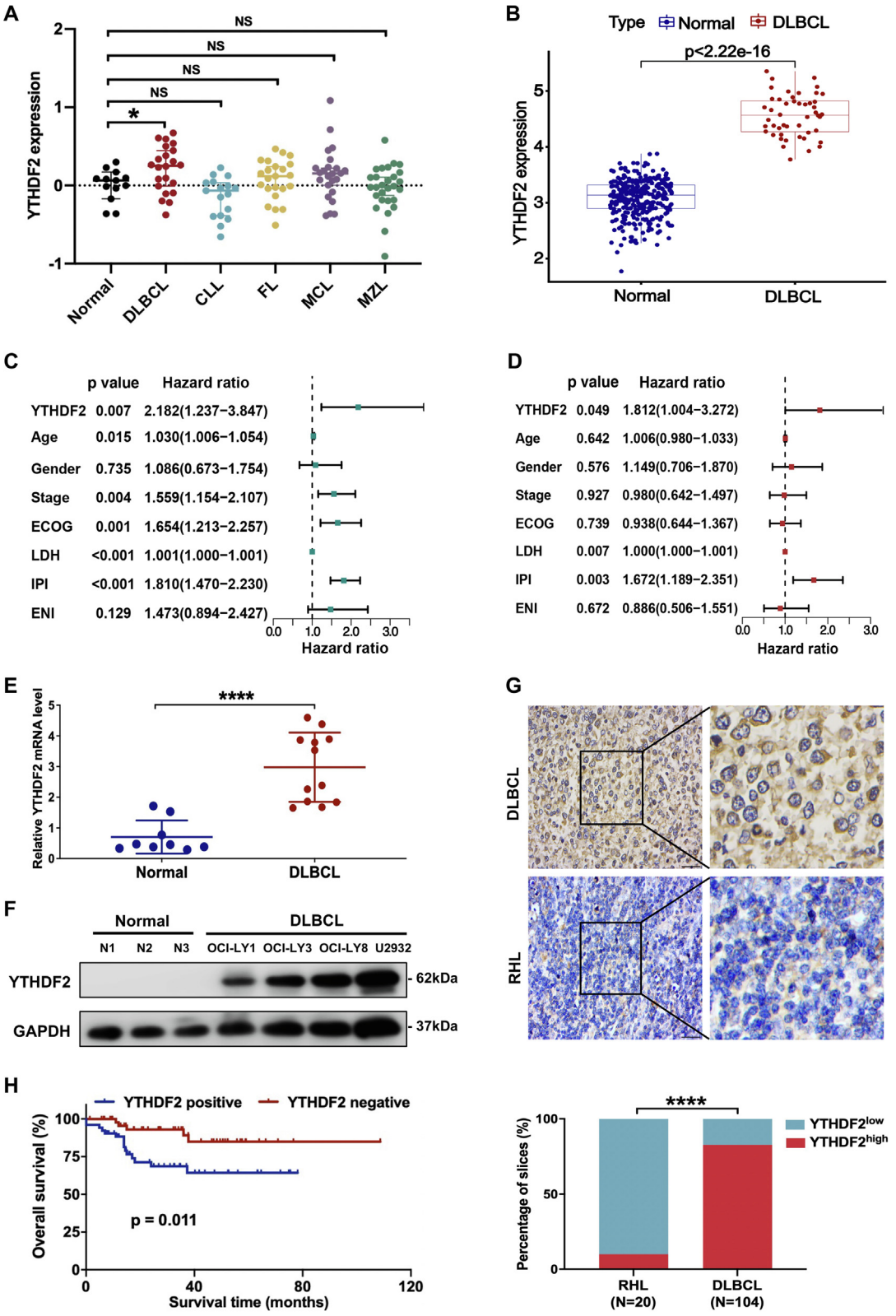

Fig. 1. YTHDF2 expression was elevated in DLBCL and indicated a poor prognosis. (A) The expression level of YTHDF2 in non-Hodgkin's lymphoma (NHL) was analyzed from GSE32018 cohort. (CLL: chronic lymphocytic leukemia, FL: follicular lymphoma, MCL: mantle cell lymphoma, MZL: marginal zone lymphoma). (B) A higher expression of YTHDF2 was observed in DLBCL samples from the TCGA dataset. (C-D) Univariate and multivariate Cox analyses of the relevance between clinicopathological signatures (containing YTHDF2) and OS of patients with DLBCL in the GSE117556 dataset. (ECOG: Eastern Cooperative Oncology Group, LDH: Lactate dehydrogenase, IPI: International Prognostic Index, ENI: Extra nodal involvement). (E) YTHDF2 mRNA level was higher in DLBCL cells (n = 4) compared to $CD19^+$ B cells (n = 3), as detected by RT-qPCR. Statistical data are presented as the mean ± SD of three independent experiments. (F) Elevated protein expression of YTHDF2 was found by western blotting analysis in DLBCL cells in contrast to $CD19^+$ B cells (N1, N2, N3). (G) Higher expression of YTHDF2 was further verified by immunohistochemistry (IHC) staining in 104 patients with DLBCL compared to patients with reactive hyperplasias of lymph nodes (RHL) (n = 20). Scale bars = 50 μm. Top: representative results; Bottom: statistical analysis of YTHDF2-positive staining in patients with DLBCL and RHL. (H) Kaplan–Meier survival analysis exhibited a positive association of YTHDF2 with poor prognosis in patients with DLBCL from IHC data. ****, $p < 0.0001$ (Student's *t*-test).

Table 1
Relevance between YTHDF2 expression and clinicopathologic characteristics of DLBCL patients.

Clinical variables	No. of patients	YTHDF2 expression		p value
		Positive	Negative	
Subtype				
GCB	38	28 (73.7%)	10(26.3%)	0.09
Non-GCB	62	54 (87.1%)	8 (12.9%)	
Age (years)				
<60	29	23 (79.3%)	6 (20.7%)	0.655
≥60	71	59 (83.1%)	12 (16.9%)	
Gender				
Male	56	48 (85.7%)	8 (14.3%)	0.275
Female	44	34 (77.3%)	10 (22.7%)	
Ann Arbor stage				
I or II	37	22 (59.5%)	15 (40.5%)	**<0.001*****
III or IV	63	60 (95.2%)	3 (48.6%)	
B symptoms				
Present	17	16 (94.1%)	1 (5.9%)	0.153
Absent	83	66 (79.5%)	17 (20.5%)	
Serum LDH				
Normal	46	34 (73.9%)	12 (26.1%)	0.052
Elevated	54	48 (88.9%)	6 (11.1%)	
Extranodal involvement				
Absent	91	73 (80.2%)	18 (19.8%)	0.527
Present	9	8 (88.9%)	1 (11.1%)	
IPI score				
0–2	49	35 (71.4%)	14 (28.6%)	**0.007****
3–5	51	47 (92.2%)	4 (7.8%)	

GCB: germinal center B cell-like, LDH: lactate dehydrogenase, IPI: International Prognostic Index. **p < 0.01, *** p < 0.001. The bold values mean statistically significant.

biological role of YTHDF2 in DLBCL progression *in vivo* (n = 5 per group) (Fig. 2N). Comparatively, overexpression of YTHDF2 dramatically accelerated DLBCL growth in SCID beige mice, as evidenced by increased tumor size and volume (Fig. 2O-P). Moreover, the expression of cell proliferation marker Ki67 was enhanced upon YTHDF2 overexpression (Fig. 2Q). The collective findings of the knockdown, knockout, and overexpression models indicated that YTHDF2 may control apoptosis, cell cycle, and proliferation, thereby potentially contributing to the progression of DLBCL.

Inhibition of YTHDF2 sensitized DLBCL cells to chemotherapeutic drugs

Given the observed resistance to chemotherapy among multiple patients diagnosed with DLBCL, the potential involvement of YTHDF2 in the development of drug resistance was determined [36]. A phase I/II clinical trial revealed a valuable application prospect with single-agent ibrutinib therapy, a selective inhibitor of Bruton's tyrosine kinase (BTK), in DLBCL [37]. Venetoclax, an oral inhibitor of Bcl-2, has exhibited a massive response to multitudinous hematologic malignancies [38–39]. Consequently, an investigation was conducted to ascertain the potential involvement of YTHDF2 in the regulation of DLBCL cell response to ibrutinib and venetoclax. A 48-hour treatment with venetoclax or ibrutinib was administered to YTHDF2 downregulated cells and control cells, respectively, and cell proliferation was then evaluated. Conspicuously, the proliferation of DLBCL cell lines with YTHDF2 knockdown was inhibited after ibrutinib or venetoclax treatment (Fig. 3A-B). Likewise, knockout of YTHDF2 significantly inhibited cell proliferation, regardless of treatment with ibrutinib or venetoclax (**Supplementary** Fig. S2L-M). The response of DLBCL cells overexpressing YTHDF2 to ibrutinib or venetoclax was also examined, and overexpression of YTHDF2 was found to facilitate cell proliferation after treatment with ibrutinib or venetoclax (Fig. 3C-D). These findings suggested that repression of YTHDF2 elevated the sensitivity of DLBCL cells to ibrutinib or venetoclax.

YTHDF2 deletion elevated endogenous ceramide levels of DLBCL cells

RNA-seq in YTHDF2 stable knockout DLBCL cells was conducted to dissect the underlying mechanism of YTHDF2. 5235 upregulated and 4890 downregulated differentially expressed genes (DEGs) were identified upon knockout of YTHDF2 in OCI-LY1 cells (Supplementary Fig. S3A). Subsequently, relevance was found between YTHDF2 and expression of 488 genes, and the top 40 genes with significant correlation were visualized by heatmap (**Supplementary** Fig. S3B). The RNA-seq analysis was followed by GO and KEGG enrichment analyses of the associated genes to investigate the function of YTHDF2 in DLBCL. The related genes were significantly enriched in the sphingolipid signaling pathway, sphingolipid metabolic process, and ceramide metabolic process (Fig. 4A-B). Since previous studies have confirmed the central role of ceramide in the sphingolipid pathway [40], a lipidomic analysis was performed to investigate whether the sphingolipid pathway, especially the ceramide metabolic process, exerted a crucial role in DLBCL cells with YTHDF2 deletion. Based on the partial least squares method-discriminant analysis (PLS-DA) model, lipid metabolite expression was significantly different between the YTHDF2 knockout and control group (Fig. 4C). Among the differentially expressed lipid molecules, 38 were overexpressed and 45 were downregulated (Supplementary Fig. S3C). Interestingly, the sphingolipids, including Ceramide (d18:1/16:0) and Ceramide (d18:2/16:0) were detected at elevated levels upon YTHDF2 deletion (Fig. 4D). Similarly, an enhanced level of total endogenous ceramide was observed in YTHDF2-deficient DLBCL cells after expanding the sample size (Fig. 4E-F).

DLBCL cells were exposed to varying concentrations of C16:0 ceramide for 24 h to conduct a more comprehensive investigation into the potential association between the dysregulation of ceramides and the progression of DLBCL. The results indicated that cell proliferation was inhibited in a concentration-dependent manner (Fig. 4G). The G2/M phase cell counts and apoptosis rates were observed to be significantly elevated upon gradually increasing ceramide concentrations as determined by flow cytometric analy-

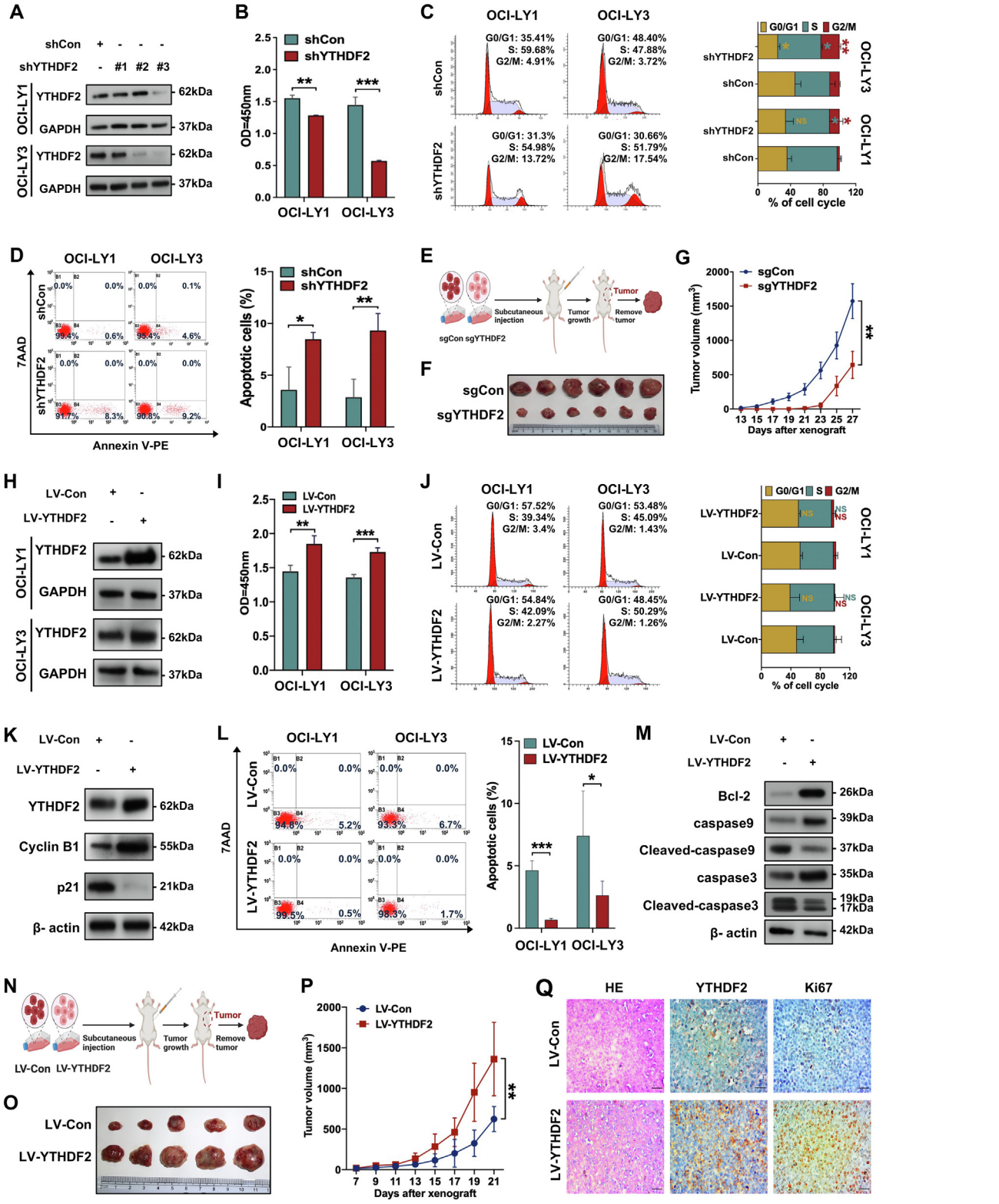

Fig. 2. YTHDF2 exerted tumor-promoting effects in DLBCL (A) The knockdown effect of YTHDF2 in OCI-LY1 and OCI-LY3 cells was assessed through protein expression of western blotting analysis. (B) YTHDF2 knockdown decreased the proliferative levels of OCI-LY1 and OCI-LY3 cells as detected by Cell Counting Kit-8 (CCK-8) assay. Results are the mean ± SD of three independent experiments. (C) Knockdown of YTHDF2-induced cell cycle arrest in the G2/M phase of OCI-LY1 and OCI-LY3 cells. Left: representative results; Right: the graph shows the mean ± SD from three independent experiments. (D) Annexin V-PE and 7AAD staining assays were utilized to measure cell apoptosis and flow cytometric analysis showed that YTHDF2 knockdown promoted apoptosis in OCI-LY1 and OCI-LY3 cells. Left: representative results; Right: the mean ± SD of three independent experiments is displayed. (E) Schematic representation of xenograft tumor model transplanted with YTHDF2 knockout or control DLBCL cells. (F-G) YTHDF2 knockout cells were utilized to establish a DLBCL mouse model (n = 6 per group). Measurement of tumor size and calculation of tumor volume every 2 days. (H) The overexpressed level of YTHDF2 in OCI-LY1 and OCI-LY3 cells was validated. (I) Overexpression of YTHDF2 increased the proliferative levels of OCI-LY1 and OCI-LY3 cells. Three independent experiments are presented as the mean ± SD. (J) The percentage of cell cycle distribution in YTHDF2-overexpressing OCI-LY1 and OCI-LY3 cells was determined through flow cytometry. Left: representative results; Right: three independent experiments are represented as the mean ± SD. (K) The expression of cell cycle proteins was determined. (L) The percentage of apoptotic cells was decreased in YTHDF2-upregulated cells, Left: representative results; Right: the mean ± SD from three independent experiments. (M) The expression of apoptotic proteins was detected upon YTHDF2 overexpression. (N) An illustration of xenograft tumor models transplanted with control or YTHDF2-overexpressing DLBCL cells. (O-P) The tumor volume with YTHDF2 overexpression in SCID mice was notably higher than that in mice injected with an empty vector (n = 5 per group). (Q) HE and IHC staining with Ki-67 and YTHDF2 in tissue sections of xenograft tumors. Scale bars = 50 μm. *, $p < 0.05$, **, $p < 0.01$, ***, $p < 0.001$ (Student's *t*-test).

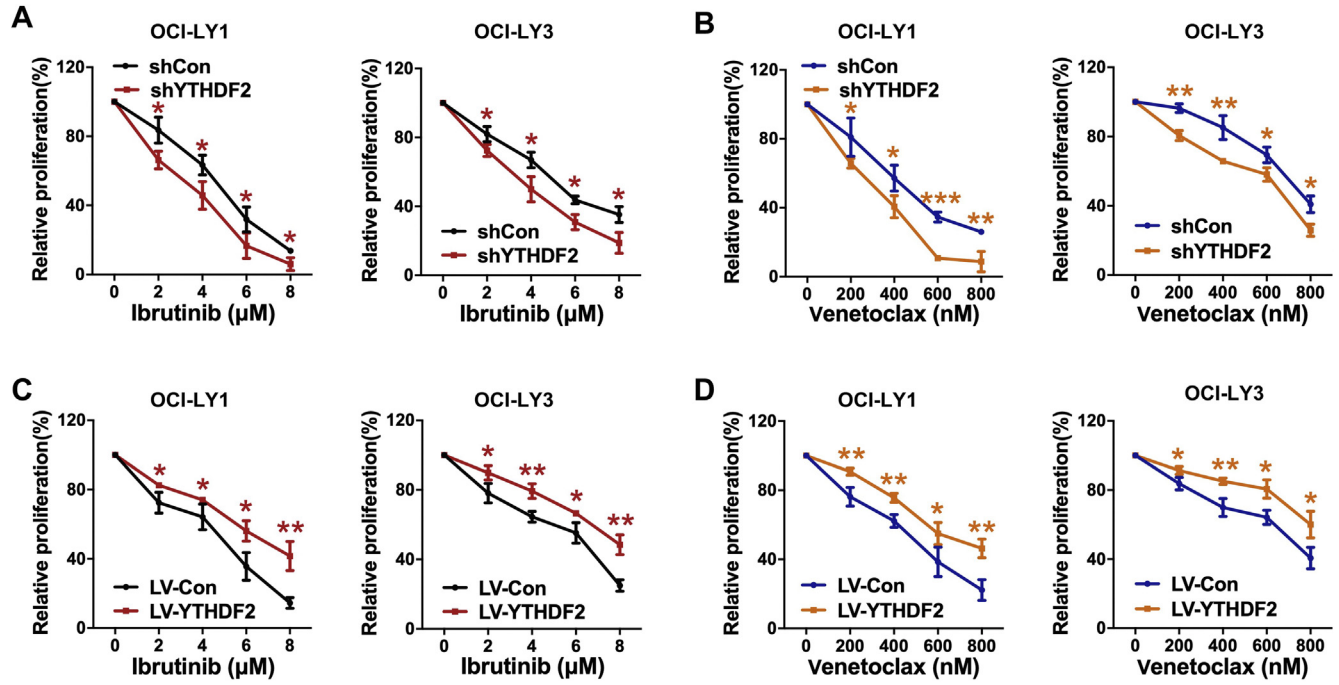

Fig. 3. YTHDF2 inhibited the sensitivity of DLBCL cells to chemotherapeutic drugs. (A-B) The proliferative levels of shYTHDF2 and shCon cells were determined after 48 h of treatment with ibrutinib or venetoclax through CCK8 assay. The data represent the mean ± SD of three independent experiments. (C-D) Administration of ibrutinib or venetoclax for 48 h in OCI-LY1 and OCI-LY3 cells with control or YTHDF2 overexpression, followed by CCK8 assay to monitor cell proliferation. The graphs show the mean ± SD from three independent experiments. *, $p < 0.05$, **, $p < 0.01$, ***, $p < 0.001$ (Student's *t*-test).

sis (Fig. 4H-I). The results suggested that ceramide possessed anti-tumor properties in DLBCL.

YTHDF2 targeted ACER2 to regulate ceramide catabolism

A correlation analysis between YTHDF2 and genes involved in ceramide metabolism from RNA-seq was performed to elucidate the precise mechanism through which YTHDF2 elicited a reduction in ceramide production. Since ceramide is modulated by its synthases and metabolic enzymes, YTHDF2 should be negatively associated with synthase and positively correlated with metabolic enzymes. Therefore, only alkaline ceramidase 2 (ACER2), which can hydrolyze ceramide to sphingosine [41], was filtered as a target gene of YTHDF2, as it was positively associated with YTHDF2 expression (Fig. 5A-B). Additionally, RT-qPCR was performed to determine mRNA levels involved in ceramide metabolism, and ACER2 still contributed the most to YTHDF2 (Fig. 5C and **Supplementary** Fig. S4A). A positive association was found between ACER2 expression and YTHDF2 expression in the TCGA dataset (Fig. 5D). Consistently, knockdown of YTHDF2 suppressed, while overexpression of YTHDF2 elevated the protein expression of ACER2 (Fig. 5E). More importantly, YTHDF2 and ACER2 mRNAs were shown to interact directly as demonstrated by RIP with an antibody against YTHDF2 followed by RT-qPCR (Fig. 5F).

Subsequently, liposomes were extracted from DLBCL cells with YTHDF2 overexpression and ACER2 knockdown to explore the potential regulatory effect of YTHDF2 on endogenous ceramide levels. The ELISA results indicated that overexpression of YTHDF2 reduced total ceramide level, while knockdown of ACER2 resulted in an increase. As anticipated, knockdown of ACER2 reversed the decrease in endogenous ceramide caused by overexpression of YTHDF2 in DLBCL cells (Fig. 5G). These results revealed that YTHDF2 promoted ACER2 expression, resulting in an imbalance of endogenous ceramide levels in DLBCL cells, and ACER2 could be a feasible downstream target of YTHDF2.

YTHDF2 facilitated ACER2 expression in an m6A-dependent manner

Given that YTHDF2 acts as an m6A binding protein, the potential regulatory role of YTHDF2 on the global m6A levels in DLBCL was investigated [42–43]. A reduced level of m6A was shown in YTHDF2-deficient DLBCL cells (Fig. 5H-I), while was elevated upon YTHDF2 overexpression (Fig. 5J). Subsequently, MeRIP-seq was performed to detect the distribution of transcriptome-wide m6A in control and YTHDF2 knockout cells. A total of 877 and 120 m6A peaks were statistically reduced and elevated, respectively, compared with control cells (**Supplementary** Fig. S4B). As expected, the m6A consensus sequence 'RRACH' was identified as highly distributed in m6A immunoprecipitated transcripts (Fig. 5K). m6A peaks were verified to be primarily enriched near the stop codons and the 3′-UTR through the analysis of m6A signal distribution (Fig. 5L). Interestingly, GO and KEGG enrichment analyses presented notable enrichment of DEGs in cellular metabolic processes and metabolic pathways, which further provided evidence that YTHDF2 promoted DLBCL progression by regulating metabolic pathways (Supplementary Fig. S4C-D). By comparing the accumulation of m6A peaks, a reduced peak was found in ACER2 mRNA on the 3′-UTR in YTHDF2 knockout cells relative to the control (Fig. 5M). Furthermore, the effects of YTHDF2 on ACER2 mRNA stability were investigated by blocking transcription with actinomycin D in control or YTHDF2-knockout OCI-LY1 cells. The decreased stability of ACER2 mRNA was observed after YTHDF2 deletion, indicating the facilitation of YTHDF2 for ACER2 mRNA stability (Fig. 5N).

Upon conducting an examination of the ACER2 mRNA sequence, it was observed that 10 sequences within the 3′-UTR exhibited concurrence with the m6A consensus sequence. The wild-type and mutant ACER2 reporter mini-genes were generated to explore the potential regulatory role of YTHDF2 on ACER2 expression through its binding to the m6A site in the 3′-UTR of ACER2 mRNA. The mutant form of ACER2 was constructed by substituting thy-

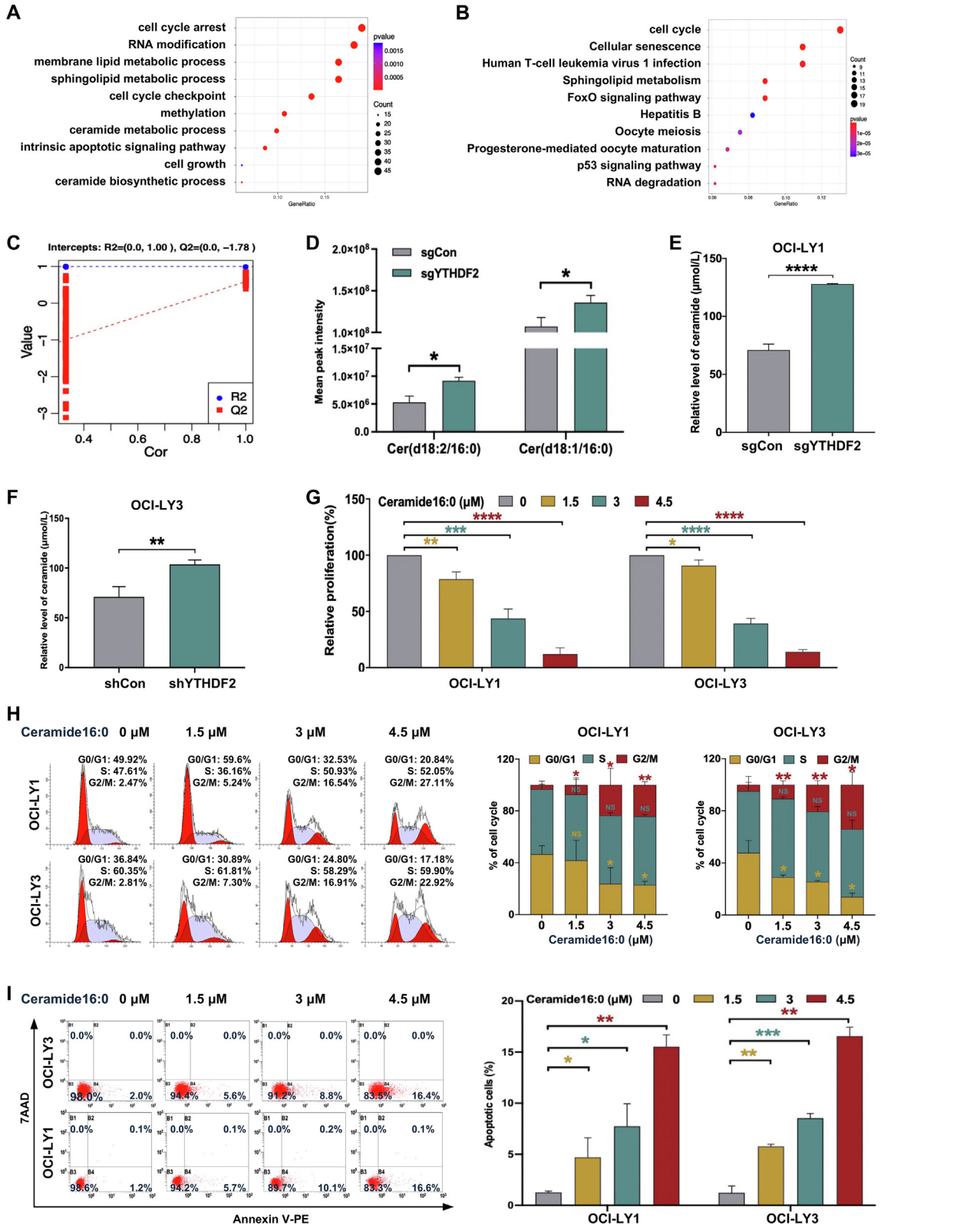

Fig. 4. YTHDF2 deletion elevated endogenous ceramide levels in DLBCL cells. (A-B) GO and KEGG enrichment analyses of the DEGs associated with YTHDF2 expression in DLBCL cells based on RNA-seq data. (C) PLS-DA analysis of lipid metabolite expression in YTHDF2 knockout and control cells. (D) Ceramide (d18:1/16:0) and Ceramide (d18:2/16:0) were increased in YTHDF2 knockout cells according to lipidomics analysis with LC-MS system. (E-F) ELISA assay showed an enhancement of global endogenous ceramide in DLBCL cells with YTHDF2 depletion. The bars show the mean ± SD of three independent experiments. (G) OCI-LY1 and OCI-LY3 cells were treated with exogenous ceramide at different concentrations for 24 h, and a CCK-8 assay was utilized to detect cell proliferation. Results represent the mean ± SD of three independent experiments. (H-I) Cell cycle and apoptosis were determined after treatment with exogenous ceramide at different concentrations for 24 h by flow cytometry. Left: representative results; Right: quantification of the cell cycle and apoptosis results are shown as the mean ± SD from three independent experiments. *, $p < 0.05$, **, $p < 0.01$, ***, $p < 0.001$, ****, $p < 0.0001$ (Student's *t*-test).

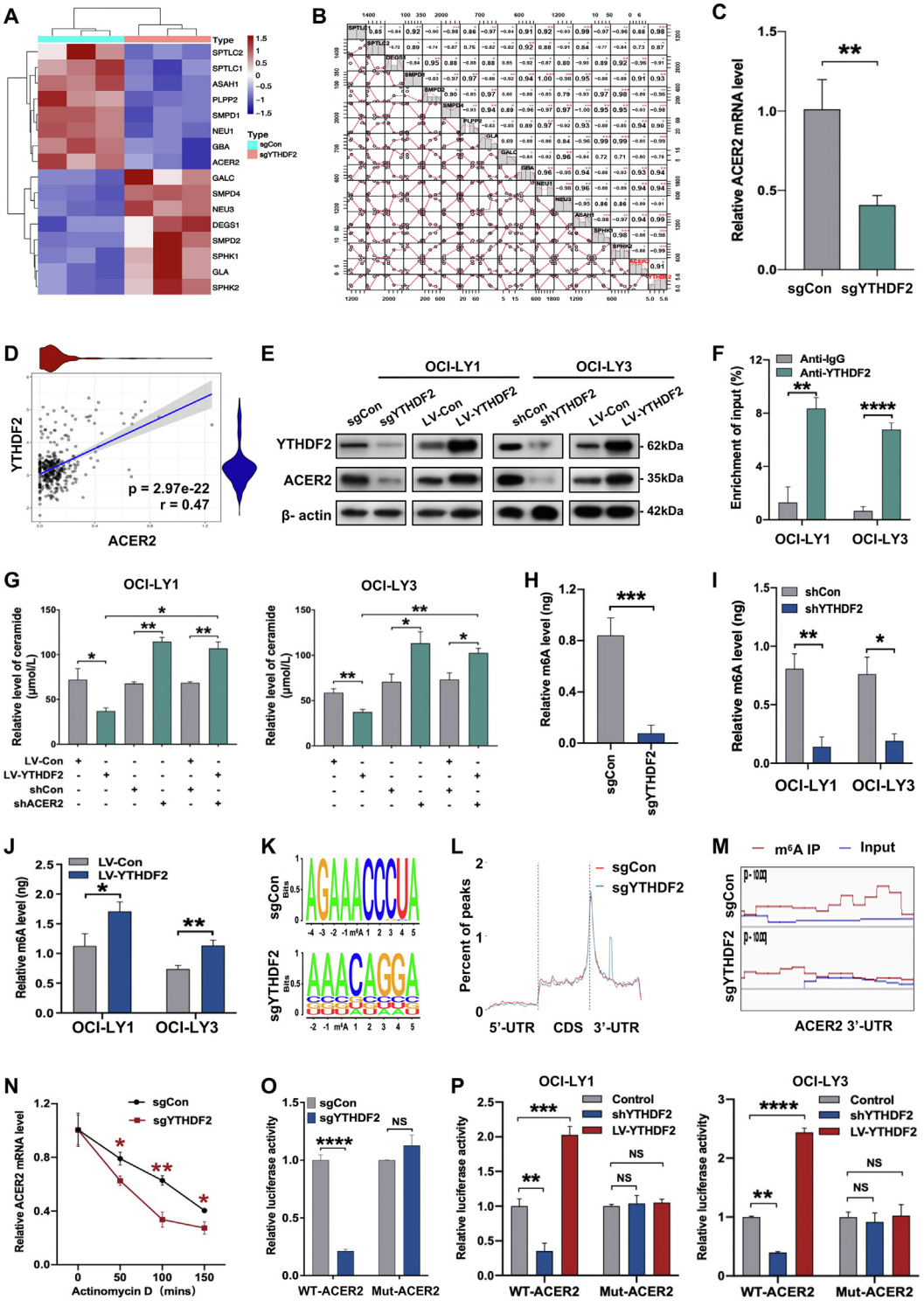

Fig. 5. YTHDF2 targeted ACER2 in an m6A-dependent manner to regulate ceramide catabolism. (A-B) The expression levels and the relevance of genes involved in ceramide metabolism and YTHDF2 in RNA-seq, verified by RT-qPCR (C) The results represent the mean ± SD of three independent experiments. (D) A positive correlation between YTHDF2 expression and ACER2 expression was determined in the TCGA dataset. (E) The positive relevance of YTHDF2 expression and ACER2 expression was further verified by western blotting analysis. (F) The enrichment of ACER2 mRNA with YTHDF2 compared to IgG in DLBCL cells was performed by RIP-qPCR analysis. Results from three independent experiments with the mean ± SD. (G) Relative ceramide concentrations of OCI-LY1 and OCI-LY3 cells in different groups were determined. Data represent the mean ± SD from three independent experiments. (H-I) Reduced m6A levels were observed in YTHDF2 knockout and knockdown DLBCL cells by a m6A RNA methylation quantification kit (mean ± SD of three independent experiments). (J) A high level of m6A was assessed in YTHDF2-overexpressing cells. Three independent experiments are shown as the mean ± SD. (K) "RRACH" was identified as the m6A consensus motif from MeRIP-seq peaks in YTHDF2 knockout and control cells. (L) Distribution of total m6A peaks across all mRNAs resulting from YTHDF2 deletion. (M) The m6A levels in the 3′-UTR of ACER2 mRNA were reduced in YTHDF2 knockout cells. (N) The mRNA level of ACER2 was detected with actinomycin-D treatment at different time points in YTHDF2 knockout and control cells. The graph represents the mean ± SD of three independent experiments. (O) Detection of luciferase activity in YTHDF2 knockout cells co-transfected with luciferase reporter GV272-ACER2 3′-UTR-WT or GV272-ACER2 3′-UTR-MUT and Renilla luciferase plasmids. The ratio of firefly luciferase to renilla luciferase represents the relative luciferase (RLU) activity. Three independent experiments are shown with the mean ± SD. (P) Luciferase activity was increased in YTHDF2-overexpressing cells transfected with luciferase reporter GV272-ACER2 3′-UTR-WT containing m6A sequences, but was diminished in YTHDF2 knockdown cells. An analysis of three independent experiments is presented with the mean ± SD. *, $p < 0.05$, **, $p < 0.01$, ***, $p < 0.001$, ****, $p < 0.0001$ (Student's *t*-test).

mine for the adenosine bases within the m6A consensus motif, effectively disrupting m6A modification. The reporter plasmids were transfected into OCI-LY1 and OCI-LY3 cells with YTHDF2 depletion or overexpression, and luciferase activity was detected upon incubation for 24 h. The luciferase activity of wild-type ACER2-fused reporter was significantly decreased in DLBCL cells with YTHDF2 deletion and enhanced in YTHDF2-overexpressing cells, whereas this inhibitory or facilitative effect was eliminated in cells with the mutant ACER2-fused reporter (Fig. 5O-P). These results indicated that YTHDF2 bound to ACER2 depended on m6A modification, thereby elevating its stability and expression in DLBCL cells.

ACER2 knockdown, inhibition of ceramide degradation, and S1P generation exerted anti-tumor effects

Given the regulatory effect exerted by YTHDF2 on ACER2 expression level, the functional role of ACER2 in DLBCL was explored. The elevated expression of ACER2 was validated in DLBCL tissues derived from TCGA (Fig. 6A). Subsequently, three ACER2 knockdown plasmids were constructed to transfect OCI-LY1 and OCI-LY3 cells. The transfection efficiency was verified at the protein level after 72 h, with shACER2#3 showing higher efficacy (Fig. 6B). Knockdown of ACER2 in DLBCL cells contributed to inhibiting cell proliferation (Fig. 6C), enhancing G2/M phase arrest (Fig. 6D), and promoting apoptosis (Fig. 6E). The upregulation of ACER2 expression by YTHDF2 prompted further investigation into the potential involvement of this regulation in the tumor-promoting function of YTHDF2 in DLBCL. As expected, the suppression of cell cycle arrest and apoptosis induced by YTHDF2 overexpression in these cells was rescued upon ACER2 knockdown (Fig. 6F-G).

As shown previously, ACER2 hydrolyzes ceramide to sphingosine, which is then catalyzed by SphK to produce S1P, thereby exerting critical roles in tumor progression [44–46]. Therefore, DLBCL cells were treated with DeM, which specifically inhibits the degradation of intracellular ceramides, and DMS, a specific inhibitor of SphK that inhibits S1P levels. After treatment with DeM or DMS for 24 h, DLBCL cell proliferation was inhibited (Fig. 7-A-B), the cell cycle was arrested in G2/M phase (Fig. 7C-D), apoptosis was facilitated (Fig. 7E-F), and it could reverse the increased cell proliferation, accelerated cycle progression, and apoptosis inhibition caused by overexpression of YTHDF2 (Fig. 7A-F). Overall, these results suggested that YTHDF2 exerted tumor-promoting effects by positively regulating ACER2 expression and S1P levels, and negatively modulating ceramide levels.

YTHDF2 activated ERK and PI3K/AKT pathways by ACER2-mediated ceramide catabolism

The above study has found that YTHDF2 inhibited intracellular ceramide levels by elevating ACER2 expression. ELISA experiments were conducted to examine the potential of YTHDF2 in increasing intracellular S1P levels via ACER2. Consistently, the results suggested that YTHDF2 overexpression enhanced the levels of endogenous S1P, while ACER2 knockdown inhibited the enhancement of endogenous S1P levels caused by YTHDF2 overexpression in DLBCL cells (Fig. 8A). Previous studies have shown that decreased levels of ceramide and increased levels of S1P would activate extracellular regulated protein kinase (ERK) and phosphatidylinositol 3-kinase (PI3K)/protein kinase B (AKT) signaling pathways, thereby accelerating cell proliferation and tumor growth. Therefore, these signaling pathway core proteins were examined in DLBCL cells treated with exogenous ceramide at different concentrations. Decreased phosphorylation levels of PI3K p110α, AKT (Ser473), and ERK were found with increased concentrations of exogenous ceramide, while total protein levels did not differ significantly (Fig. 8B).

The phosphorylation levels of core proteins in these pathways were detected to investigate whether YTHDF2 regulates the ERK and PI3K/AKT pathways. As expected, YTHDF2 deletion suppressed the phosphorylation of ERK, PI3K p110α, and AKT (Ser473), suggesting inhibition of the ERK and PI3K/AKT pathways activation (Fig. 8C). Conversely, overexpression of YTHDF2 in DLBCL cells enhanced phosphorylation of ERK, PI3K p110α, and AKT (Ser473) (Fig. 8C). These findings have instigated subsequent investigations into the potential activation of the ERK and PI3K/AKT pathways by YTHDF2 through the promotion of ACER2 expression in DLBCL cells. A shACER2 plasmid or a control plasmid was injected into DLBCL cells. Consistent with the increased concentrations of ceramide, ERK, PI3K p110α, and AKT (Ser473) phosphorylation levels were decreased in DLBCL cells with ACER2 knockdown (Fig. 8D). Moreover, knockdown of ACER2 reversed the elevated phosphorylation levels of ERK, PI3K p110α, and AKT (Ser473) caused by YTHDF2 overexpression (Fig. 8D). Collectively, these findings revealed that YTHDF2 facilitated ACER2 expression to inhibit endogenous ceramide levels, thereby activating the ERK and PI3K/AKT pathways in DLBCL cells.

Discussion

m6A is the most abundant chemical modification among the over 100 different RNA modifications in eukaryotes [47]. However, RNA modifications are still largely unidentified from the biological perspective and their mechanisms. There is existing evidence supporting that YTHDF2 played an important role in leukemia, but few studies have been conducted on other hematological malignancies, including DLBCL [48]. This study presents novel findings indicating a significant association between elevated YTHDF2 expression in DLBCL and worse prognosis. YTHDF2 bound to m6A sites in the ACER2 mRNA 3′-UTR to maintain its stability and expression, thereby contributing to endogenous ceramide hydrolysis. Repression of YTHDF2 executed its anti-tumor effect of restricting cell proliferation, facilitating cell cycle arrest and apoptosis through suppressing ACER2-mediated ceramide catabolism, thereby promoting ceramide accumulation and reducing S1P levels, which in turn inhibited the activation of the ERK and PI3K/AKT pathways. Treatment with exogenous ceramide or depletion of ACER2 significantly inhibited DLBCL progression. Therefore, these findings shed light on a novel epigenetic variation story that contributed to the investigation of DLBCL progression.

Previous studies have revealed that YTHDF2 accelerates the progression of lung adenocarcinoma [9], pancreatic cancer [49], acute myeloid leukemia [50], and liver cancer [51]. There is a lack of research investigating the roles and potential mechanisms associated with YTHDF2 in DLBCL. This study revealed that YTHDF2 overexpression was correlated with a poorer prognosis of DLBCL patients and exerted an independent prognostic role. This study functionally validated that YTHDF2 played a tumor-promoting role in DLBCL through lentiviral-mediated gene knockdown, CRISPR/Cas9 gene knockout, and lentiviral-based gene overexpression. Suppression of YTHDF2 demonstrated its anti-tumor effects by repressing cell proliferation, arresting cell cycle in the G2/M phase, facilitating apoptosis and chemo-sensitivity in DLBCL cells *in vitro*, and suppressing DLBCL tumor growth *in vivo*. Collectively, these results provided evidence that YTHDF2 contributed to DLBCL progression.

Previous studies have indicated the core role of ceramide in the sphingolipid pathway for it functions as a cornerstone for synthesizing complex sphingolipids [52–53]. The RNA-seq analysis demonstrated that YTHDF2 mediated sphingolipid metabolism

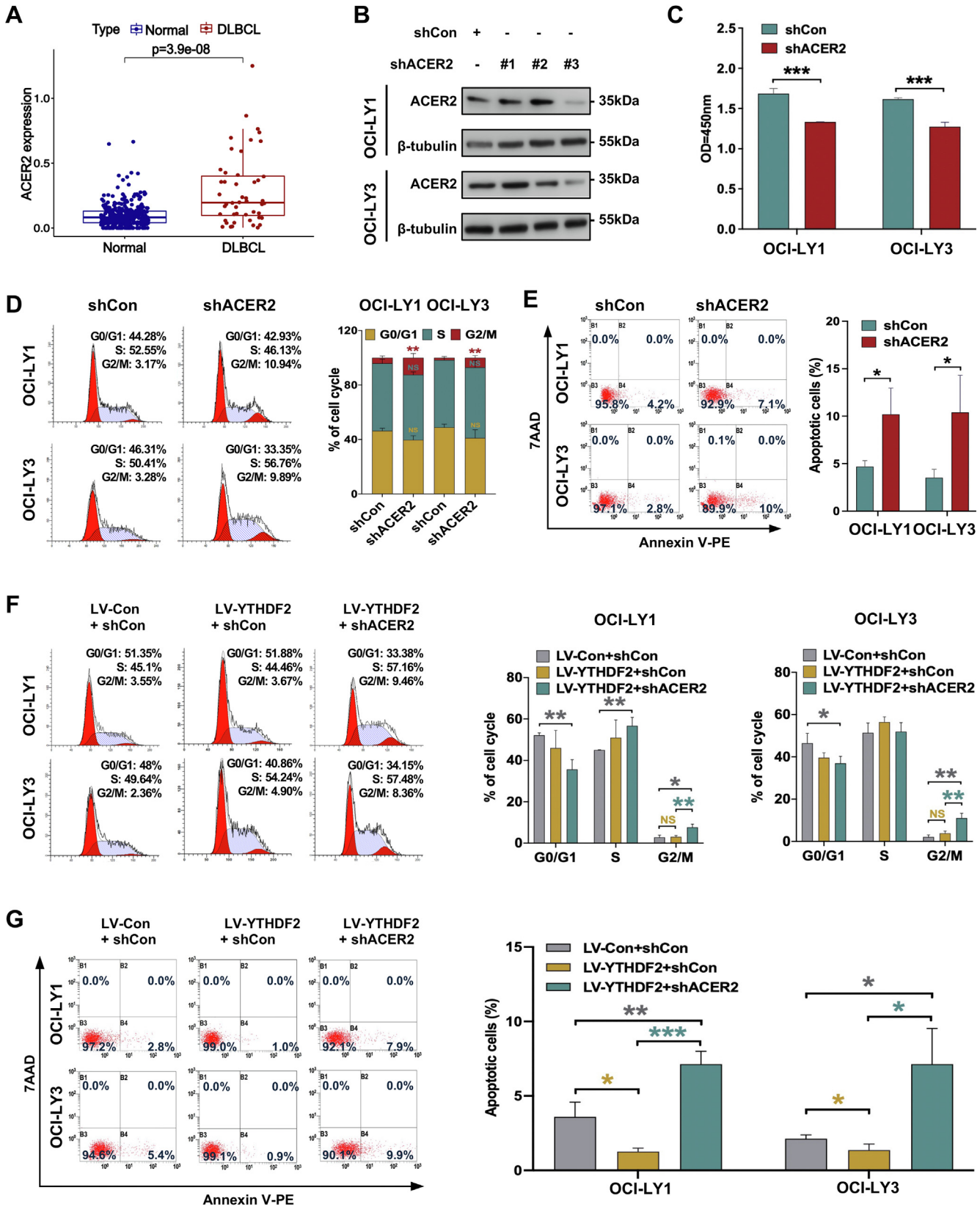

Fig. 6. ACER2 knockdown suppressed DLBCL tumorigenesis. (A) ACER2 was upregulated in DLBCL through the analysis of the TCGA dataset. (B) The transfected effect of ACER2 shRNA plasmid on YTHDF2-depleted cells was detected. (C) Knockdown of ACER2 inhibited DLBCL cell proliferation. The bars show the mean ± SD of three independent experiments. (D-E) ACER2 knockdown induced cell cycle arrest in the G2/M phase and promoted apoptosis in DLBCL. Left: Representative results for the distributions of cell cycle and apoptosis of DLBCL cells. Right: Quantification of the results is shown as the mean ± SD from three independent experiments. (F-G) Left: Representative results for the distributions of cell cycle and apoptosis of DLBCL cells with ACER2 knockdown or both ACER2 knockdown and YTHDF2 overexpression. Right: Quantification of the results is shown as the mean ± SD from three independent experiments. *, $p < 0.05$, **, $p < 0.01$, ***, $p < 0.001$ (Student's *t*-test).

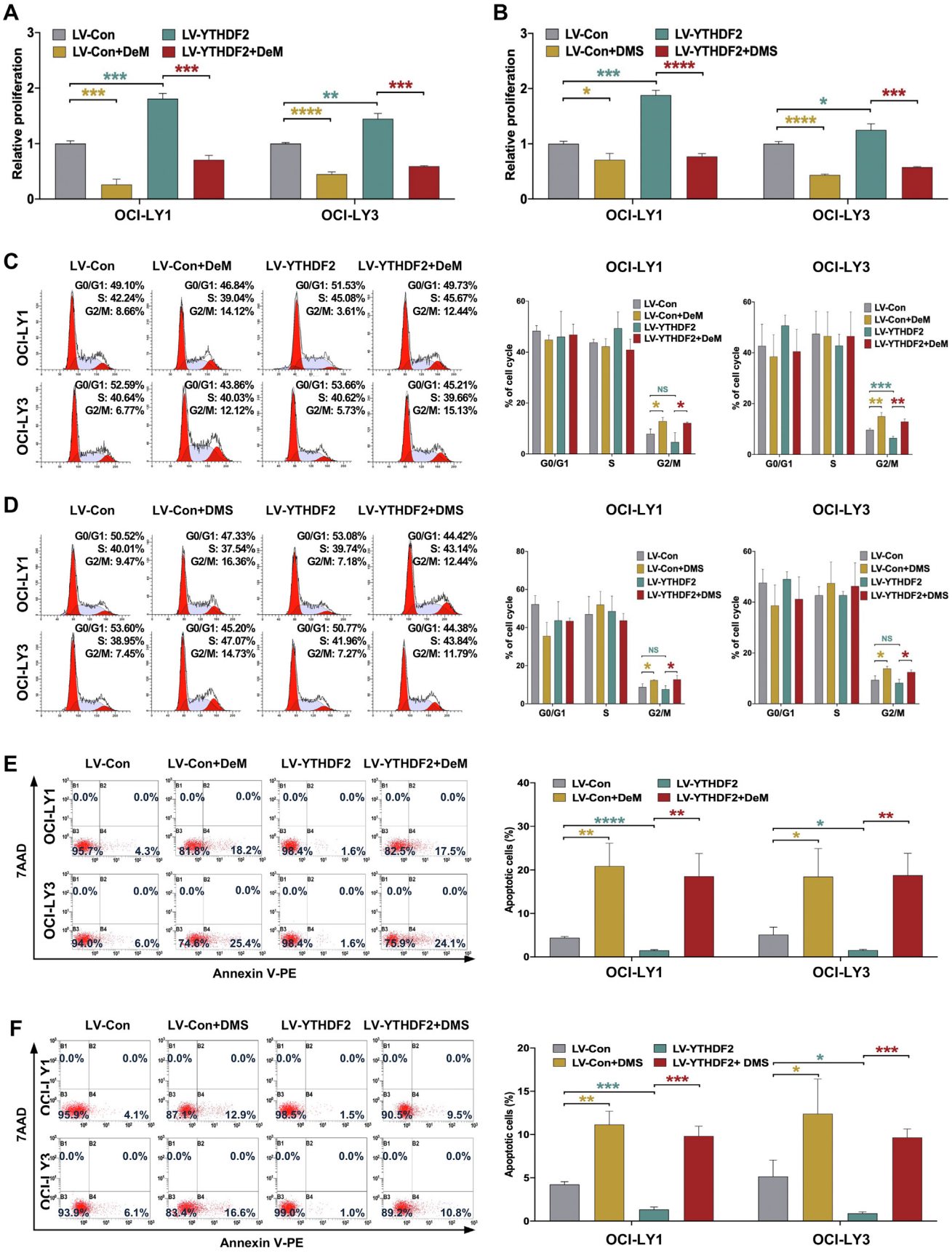

Fig. 7. Inhibition of ceramide degradation and S1P generation exerted anti-tumor effects. (A-B) The proliferation of DLBCL cells was assessed by CCK-8 assay after 24 h of treatment with ceramidase inhibitor DeM (A) or sphingosine kinase inhibitor DMS (B). The mean ± SD is shown for three independent experiments. (C-F) Treatment with DeM or DMS for 24 h inhibited DLBCL cells arrested the cell cycle in the G2/M phase, facilitated apoptosis, and reversed the accelerated cycle progression and apoptosis suppression elicited by YTHDF2 overexpression. Left: representative pictures; Right: quantitative data from three independent experiments with the mean ± SD. *, $p < 0.05$, **, $p < 0.01$, ***, $p < 0.001$, ****, $p < 0.0001$ (Student's *t*-test).

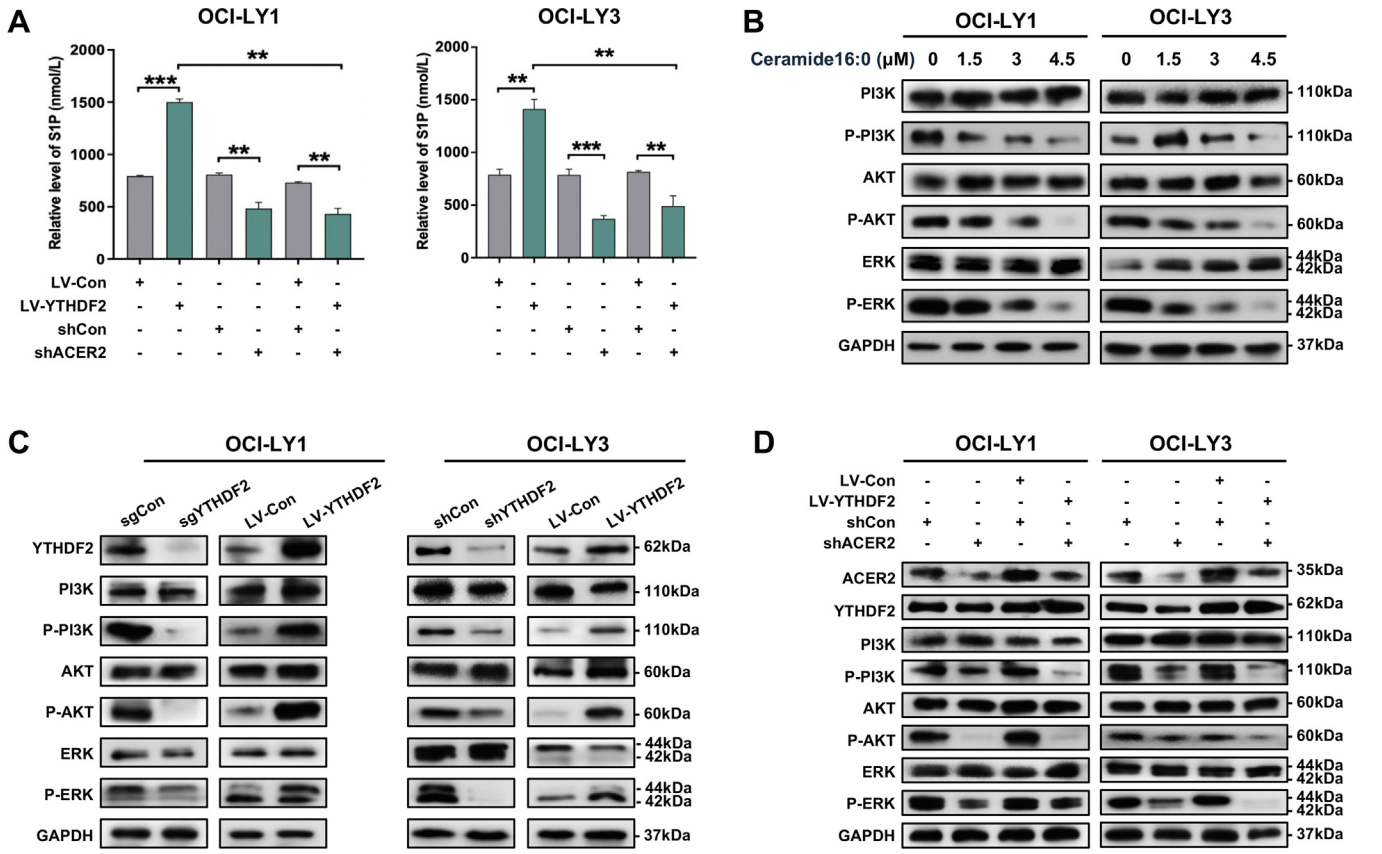

Fig. 8. YTHDF2 activated the ERK and PI3K/AKT pathways through ceramide catabolism regulated by ACER2. (A) Relative S1P concentrations were detected by ELISA in DLBCL cells with ACER2 knockdown and YTHDF2 overexpression. The graphs present the mean ± SD from three independent experiments. (B) OCI-LY1 and OCI-LY3 cells were harvested upon treatment with different concentrations of ceramide and the phosphorylated and total protein levels of PI3K, AKT, and ERK were detected by western blotting. (C) Suppressed activation of the ERK and PI3K/AKT pathways was found in YTHDF2 knockout DLBCL cells and a contrary result was shown in DLBCL cells overexpressing YTHDF2. (D) Knockdown of ACER2 further inhibited the activation of the ERK and PI3K/AKT pathways in DLBCL cells with YTHDF2 overexpression. *, $p < 0.05$, **, $p < 0.01$, ***, $p < 0.001$, ****, $p < 0.0001$ (Student's *t*-test).

and ceramide metabolic process. Known as a "tumor suppressor lipid", ceramide energetically enhances signaling events such as cell cycle arrest, apoptosis, and autophagic response [54]. In addition, stimulating *de novo*-synthesized ceramide resulted in the initiation of autophagy in DLBCL cells [55]. This study demonstrated that YTHDF2 reduced endogenous ceramide levels in DLBCL cells. Additionally, introduction of exogenous ceramide inhibited the malignant phenotype of DLBCL cells *in vitro*. These findings indicated the potential of ceramide in the therapeutic intervention of DLBCL through regulation of YTHDF2.

Ceramide levels in cells were reported to be controlled by the balance of anabolism and catabolism [56]. This study observed that ACER2, an enzyme that hydrolyzes ceramides to sphingosines, contributed the most to ceramide levels in cells with YTHDF2 deletion. ACER2 repression enhanced endogenous ceramide levels and inhibited the decrease in ceramide levels elicited by YTHDF2 overexpression, providing evidence for ACER2 as a crucial factor in the regulatory mechanism of YTHDF2 on endogenous ceramides. Accumulating studies have indicated that numerous cancer cells express ACER2, which participates in proliferation, autophagy, apoptosis, and DNA damage response [23,57]. This study showed that ACER2 functioned as a tumor-promoting factor in DLBCL and the tumor suppressive effect exerted by YTHDF2 deletion was dependent on the regulation of ACER2.

Despite being the most prevalent epigenetic signature on eukaryotic mRNAs, the biological functions and regulatory mechanisms of m6A modification could exhibit divergence in response to varying situations or in relation to distinct genes [58]. Growing evidence has revealed that the m6A modification recognized by YTHDF2 is most frequently situated in the 3′-UTR of mRNA, resulting in transcript degradation [59–60]. Nevertheless, it remains to be fully investigated whether YTHDF2-recognized m6A modification facilitates gene expression. It was revealed that m6A modification of 6-phosphogluconate dehydrogenase (6PGD) in the 3′-UTR accelerated protein translation, which was determined by YTHDF2 [9]. The high m6A level might result from the delay in mRNA degradation, leading to the retention of transcripts modified by m6A to YTHDF2-deficient cells, thereby increasing its deposition. However, the mechanism of the decline in m6A levels mediated by YTHDF2 depletion remains unclear. YTHDF2 was proven to be bound to the m6A site on the 5′-UTR of OCT4 mRNA to promote its translation [51]. The above evidence demonstrated that YTHDF2 regulated m6A modification through divergent mechanisms. The current study revealed that YTHDF2 increased global m6A levels in DLBCL cells and bound to the m6A sites on ACER2 mRNA 3′-UTR, thereby enhancing ACER2 stability and expression. Further studies should be specific to the initiation and extension of translation to dissect the mechanism by which YTHDF2-recognized m6A modifications facilitate protein expression.

ACER2 functions to catalyze ceramides into sphingosines, which in turn are phosphorylated to yield S1P, a biologically active lipid that promotes survival and proliferation [23]. Decreased ceramide and increased S1P accelerate cell proliferation and tumor growth by activating the AKT and ERK pathways [19,61]. This study illustrated that the levels of S1P in DLBCL cells were positively regulated by YTHDF2 overexpression and negatively regulated by

ACER2 inhibition. Moreover, inhibition of intracellular ceramide degradation and S1P generation exerted tumor suppressive effects in DLBCL by inhibiting cell proliferation, promoting cell cycle arrest, and inducing apoptosis. This study also found that YTHDF2 promoted the phosphorylation of ERK and PI3K p110α and its downstream targets AKT to activate the ERK and PI3K/AKT pathways, while treatment with exogenous ceramide and ACER2 inhibition suppressed the ERK and PI3K/AKT pathways activation induced by YTHDF2 overexpression. Previous studies indicated that insensitivity to BTK inhibition leads to poor clinical outcomes correlated with the ERK pathway activation [62]. BTK activation in cancer cells contributes to downstream PI3K activation [63]. Bcl-2 family proteins are effectors of the ERK and PI3K/AKT signaling cascades [64]. This study demonstrated that YTHDF2 repression could sensitize DLBCL cells to ibrutinib or venetoclax, which may be achieved by reprogramming target gene expression through repressing activation of ERK and PI3K-Akt signaling cascades, providing further evidence for previous findings. These findings demonstrated that the YTHDF2-ACER2-S1P/ceramide axis could be a crucial cornerstone in DLBCL tumorigenesis by regulating the ERK and PI3K/AKT pathways.

Conclusions

The current study demonstrated that YTHDF2 contributed to DLBCL progression and poor prognosis, and bound to m6A sites on 3′-UTR of ACER2 mRNA to enhance ACER2 stability and expression. The accumulations of ACER2 triggered endogenous ceramide catabolism and increased the S1P levels to activate PI3K/AKT and ERK pathways. These findings revealed a novel mechanism for epigenetic regulation of ceramide catabolism by YTHDF2 in DLBCL progression and highlighted the potential of YTHDF2 as a therapeutic target and predictor for DLBCL.

Author statement

X.Z. and X.W. conceived, directed, and supervised the study and critically revised and approved the manuscript. X.C. performed the experiment, analyzed the data, and wrote the manuscript. T.L., M. D., Y.C., and Z.Y. participated in the experiments and analyzed the data. All authors read and approved the final manuscript.

Compliance with Ethics requirements

The study was approved by the Medical Ethics Committee of Shandong Provincial Hospital. All healthy volunteers and patients providing clinical specimens signed the written informed consent form. All procedures were carried out in accordance with the principles of Declaration of Helsinki. All animal experiments were conducted according to the protocols approved by the Institutional Animal Care and Research Advisory Committee of Shandong Provincial Hospital.

Declaration of Competing Interest

The authors declare that they have no known competing financial interests or personal relationships that could have appeared to influence the work reported in this paper.

Acknowledgments

This study was supported by National Natural Science Foundation (No.82270200, No.82170189, No.82070203, No.81800194, No.81770210); Key Research and Development Program of Shandong Province (No.2018CXGC1213); China Postdoctoral Science Foundation (No.2021T1404223); Translational Research Grant of NCRCH (No.2021WWB02, No.2020ZKMB01); Shandong Provincial Natural Science Foundation (ZR2021YQ51); Taishan Scholars Program of Shandong Province; Shandong Provincial Engineering Research Center of Lymphoma; Academic Promotion Programme of Shandong First Medical University (No. 2019QL018).

Appendix A. Supplementary material

Supplementary data to this article can be found online at https://doi.org/10.1016/j.jare.2023.10.010.

References

[1] Mottok A, Hung SS, Chavez EA, Woolcock B, Telenius A, Chong LC, et al. Integrative genomic analysis identifies key pathogenic mechanisms in primary mediastinal large B-cell lymphoma. Blood 2019;134(10):802–13.
[2] Sehn LH, Salles G. Diffuse Large B-Cell Lymphoma. N Engl J Med 2021;384(9):842–58.
[3] Hayden AR, Tonseth P, Lee DG, Villa D, Gerrie AS, Scott DW, et al. Outcome of primary mediastinal large B-cell lymphoma using R-CHOP: impact of a PET-adapted approach. Blood 2020;136(24):2803–11.
[4] Miao Y, Medeiros LJ, Li Y, Li J, Young KH. Genetic alterations and their clinical implications in DLBCL. Nat Rev Clin Oncol 2019;16(10):634–52.
[5] Clozel T, Yang S, Elstrom RL, Tam W, Martin P, Kormaksson M, et al. Mechanism-based epigenetic chemosensitization therapy of diffuse large B-cell lymphoma. Cancer Discov 2013;3(9):1002–19.
[6] Wang X, Zhao BS, Roundtree IA, Lu Z, Han D, Ma H, et al. N(6)-methyladenosine Modulates Messenger RNA Translation Efficiency. Cell 2015;161(6):1388–99.
[7] Li HB, Tong J, Zhu S, Batista PJ, Duffy EE, Zhao J, et al. m(6)A mRNA methylation controls T cell homeostasis by targeting the IL-7/STAT5/SOCS pathways. Nature 2017;548(7667):338–42.
[8] Cai Y, Feng R, Lu T, Chen X, Zhou X, Wang X. Novel insights into the m(6)A-RNA methyltransferase METTL3 in cancer. Biomark Res 2021;9(1):27.
[9] Sheng H, Li Z, Su S, Sun W, Zhang X, Li L, et al. YTH domain family 2 promotes lung cancer cell growth by facilitating 6-phosphogluconate dehydrogenase mRNA translation. Carcinogenesis 2020;41(5):541–50.
[10] Chen X, Zhou X, Wang X. m(6)A binding protein YTHDF2 in cancer. Exp Hematol Oncol 2022;11(1):21.
[11] Fang R, Chen X, Zhang S, Shi H, Ye Y, Shi H, et al. EGFR/SRC/ERK-stabilized YTHDF2 promotes cholesterol dysregulation and invasive growth of glioblastoma. Nat Commun 2021;12(1):177.
[12] Yu J, She Y, Yang L, Zhuang M, Han P, Liu J, et al. The m(6) A Readers YTHDF1 and YTHDF2 Synergistically Control Cerebellar Parallel Fiber Growth by Regulating Local Translation of the Key Wnt5a Signaling Components in Axons. Adv Sci (Weinh) 2021;8(22):e2101329.
[13] Chen X, Lu T, Cai Y, Han Y, Ding M, Chu Y, et al. KIAA1429-mediated m6A modification of CHST11 promotes progression of diffuse large B-cell lymphoma by regulating Hippo-YAP pathway. Cell Mol Biol Lett 2023;28(1):32.
[14] Wang S, Chen S, Sun J, Han P, Xu B, Li X, et al. m(6)A modification-tuned sphingolipid metabolism regulates postnatal liver development in male mice. Nat Metab 2023;5(5):842–60.
[15] Lu T, Shi L, Shi G, Cai Y, Hu S, Liu J, et al. Derivation and validation of a lipid-covered prognostic model for mature T-cell lymphomas. Cancer Cell Int 2021;21(1):348.
[16] Kapadia B, Nanaji NM, Bhalla K, Bhandary B, Lapidus R, Beheshti A, et al. Fatty Acid Synthase induced S6Kinase facilitates USP11-eIF4B complex formation for sustained oncogenic translation in DLBCL. Nat Commun 2018;9(1):829.
[17] Hannun YA, Obeid LM. Principles of bioactive lipid signalling: lessons from sphingolipids. Nat Rev Mol Cell Biol 2008;9(2):139–50.
[18] Lewis AC, Pope VS, Tea MN, Li M, Nwosu GO, Nguyen TM, et al. Ceramide-induced integrated stress response overcomes Bcl-2 inhibitor resistance in acute myeloid leukemia. Blood 2022;139(26):3737–51.
[19] Xun C, Chen MB, Qi L, Tie-Ning Z, Peng X, Ning L, et al. Targeting sphingosine kinase 2 (SphK2) by ABC294640 inhibits colorectal cancer cell growth in vitro and in vivo. J Exp Clin Cancer Res 2015;34:94.
[20] Vu TM, Ishizu AN, Foo JC, Toh XR, Zhang F, Whee DM, et al. Mfsd2b is essential for the sphingosine-1-phosphate export in erythrocytes and platelets. Nature 2017;550(7677):524–8.
[21] Papsdorf K, Brunet A. Linking Lipid Metabolism to Chromatin Regulation in Aging. Trends Cell Biol 2019;29(2):97–116.
[22] Cheng JC, Bai A, Beckham TH, Marrison ST, Yount CL, Young K, et al. Radiation-induced acid ceramidase confers prostate cancer resistance and tumor relapse. J Clin Invest 2013;123(10):4344–58.
[23] Xu R, Garcia-Barros M, Wen S, Li F, Lin CL, Hannun YA, et al. Tumor suppressor p53 links ceramide metabolism to DNA damage response through alkaline ceramidase 2. Cell Death Differ 2018;25(5):841–56.
[24] Fyrst H, Saba JD. An update on sphingosine-1-phosphate and other sphingolipid mediators. Nat Chem Biol 2010;6(7):489–97.
[25] Park J, Euhus DM, Scherer PE. Paracrine and endocrine effects of adipose tissue on cancer development and progression. Endocr Rev 2011;32(4):550–70.

[26] Zhao Y, Yang J, Liu J, Cai Y, Han Y, Hu S, et al. Inhibition of Polo-like kinase 4 induces mitotic defects and DNA damage in diffuse large B-cell lymphoma. Cell Death Dis 2021;12(7):640.
[27] Yang J, Li Y, Zhang Y, Fang X, Chen N, Zhou X, et al. Sirt6 promotes tumorigenesis and drug resistance of diffuse large B-cell lymphoma by mediating PI3K/Akt signaling. J Exp Clin Cancer Res 2020;39(1):142.
[28] Zhou X, Chen N, Xu H, Zhou X, Wang J, Fang X, et al. Regulation of Hippo-YAP signaling by insulin-like growth factor-1 receptor in the tumorigenesis of diffuse large B-cell lymphoma. J Hematol Oncol 2020;13(1):77.
[29] An Y, Chang W, Wang W, Wu H, Pu K, Wu A, et al. A novel tetrapeptide fluorescence sensor for early diagnosis of prostate cancer based on imaging Zn (2+) in healthy versus cancerous cells. J Adv Res 2020;24:363–70.
[30] Zhou X, Fang X, Jiang Y, Geng L, Li X, Li Y, et al. Klotho, an anti-aging gene, acts as a tumor suppressor and inhibitor of IGF-1R signaling in diffuse large B cell lymphoma. J Hematol Oncol 2017;10(1):37.
[31] Zheng K, Chen Z, Feng H, Chen Y, Zhang C, Yu J, et al. Sphingomyelin synthase 2 promotes an aggressive breast cancer phenotype by disrupting the homoeostasis of ceramide and sphingomyelin. Cell Death Dis 2019;10(3):157.
[32] Liu J, Han Y, Hu S, Cai Y, Yang J, Ren S, et al. Circulating Exosomal MiR-107 Restrains Tumorigenesis in Diffuse Large B-Cell Lymphoma by Targeting 14-3-3η. Front Cell Dev Biol 2021;9:667800.
[33] Lei Q, Yu Z, Li H, Cheng J, Wang Y. Fatty acid-binding protein 5 aggravates pulmonary artery fibrosis in pulmonary hypertension secondary to left heart disease via activating wnt/beta-catenin pathway. J Adv Res 2022;40:197–206.
[34] Qian Z, Ye J, Li J, Che Y, Yu W, Xu P, et al. Decrotonylation of AKT1 promotes AKT1 phosphorylation and activation during myogenic differentiation. J Adv Res 2023;50:117–33.
[35] Zhang P, He Q, Wang Y, Zhou G, Chen Y, Tang L, et al. Protein C receptor maintains cancer stem cell properties via activating lipid synthesis in nasopharyngeal carcinoma. Signal Transduct Target Ther 2022;7(1):46.
[36] Jain N, Singh S, Laliotis G, Hart A, Muhowski E, Kupcova K, et al. Targeting phosphatidylinositol 3 kinase-β and -δ for Bruton tyrosine kinase resistance in diffuse large B-cell lymphoma. Blood Adv 2020;4(18):4382–92.
[37] Goy A, Ramchandren R, Ghosh N, Munoz J, Morgan DS, Dang NH, et al. Ibrutinib plus lenalidomide and rituximab has promising activity in relapsed/refractory non-germinal center B-cell-like DLBCL. Blood 2019;134(13):1024–36.
[38] Phillips DC, Jin S, Gregory GP, Zhang Q, Xue J, Zhao X, et al. A novel CDK9 inhibitor increases the efficacy of venetoclax (ABT-199) in multiple models of hematologic malignancies. Leukemia 2020;34(6):1646–57.
[39] Fischer MA, Friedlander SY, Arrate MP, Chang H, Gorska AE, Fuller LD, et al. Venetoclax response is enhanced by selective inhibitor of nuclear export compounds in hematologic malignancies. Blood Adv 2020;4(3):586–98.
[40] Zhang X, Zhang Y, Wang P, Zhang SY, Dong Y, Zeng G, et al. Adipocyte Hypoxia-Inducible Factor 2alpha Suppresses Atherosclerosis by Promoting Adipose Ceramide Catabolism. Cell Metab 2019;30(5):937–51 e5.
[41] de Groot T, Ebert LK, Christensen BM, Andralojc K, Cheval L, Doucet A, et al. Identification of Acer2 as a First Susceptibility Gene for Lithium-Induced Nephrogenic Diabetes Insipidus in Mice. J Am Soc Nephrol 2019;30 (12):2322–36.
[42] Hsu PJ, Zhu Y, Ma H, Guo Y, Shi X, Liu Y, et al. Ythdc2 is an N(6)-methyladenosine binding protein that regulates mammalian spermatogenesis. Cell Res 2017;27(9):1115–27.
[43] Chen X, Gong W, Shao X, Shi T, Zhang L, Dong J, et al. METTL3-mediated m(6)A modification of ATG7 regulates autophagy-GATA4 axis to promote cellular senescence and osteoarthritis progression. Ann Rheum Dis 2022;81(1):87–99.
[44] Zhang Y, Cheng L, Shi X, Song Y, Chen XY, Chen MB, et al. The sphingosine kinase inhibitor SKI-V suppresses cervical cancer cell growth. Int J Biol Sci 2022;18(7):2994–3005.
[45] Diab KJ, Adamowicz JJ, Kamocki K, Rush NI, Garrison J, Gu Y, et al. Stimulation of sphingosine 1-phosphate signaling as an alveolar cell survival strategy in emphysema. Am J Respir Crit Care Med 2010;181(4):344–52.
[46] Venkata JK, An N, Stuart R, Costa LJ, Cai H, Coker W, et al. Inhibition of sphingosine kinase 2 downregulates the expression of c-Myc and Mcl-1 and induces apoptosis in multiple myeloma. Blood 2014;124(12):1915–25.
[47] Xuan JJ, Sun WJ, Lin PH, Zhou KR, Liu S, Zheng LL, et al. RMBase v2.0: deciphering the map of RNA modifications from epitranscriptome sequencing data. Nucleic Acids Res 2018;46(D1):D327–34.
[48] Qing Y, Dong L, Gao L, Li C, Li Y, Han L, et al. R-2-hydroxyglutarate attenuates aerobic glycolysis in leukemia by targeting the FTO/m(6)A/PFKP/LDHB axis. Mol Cell 2021;81(5).
[49] Chen Y, Ling Z, Cai X, Xu Y, Lv Z, Man D, et al. Activation of YAP1 by N6-Methyladenosine-Modified circCPSF6 Drives Malignancy in Hepatocellular Carcinoma. Cancer Res 2022;82(4):599–614.
[50] Paris J, Morgan M, Campos J, Spencer GJ, Shmakova A, Ivanova I, et al. Targeting the RNA m(6)A Reader YTHDF2 Selectively Compromises Cancer Stem Cells in Acute Myeloid Leukemia. Cell Stem Cell 2019;25(1).
[51] Zhang C, Huang S, Zhuang H, Ruan S, Zhou Z, Huang K, et al. YTHDF2 promotes the liver cancer stem cell phenotype and cancer metastasis by regulating OCT4 expression via m6A RNA methylation. Oncogene 2020;39(23):4507–18.
[52] Orsini M, Chateauvieux S, Rhim J, Gaigneaux A, Cheillan D, Christov C, et al. Sphingolipid-mediated inflammatory signaling leading to autophagy inhibition converts erythropoiesis to myelopoiesis in human hematopoietic stem/progenitor cells. Cell Death Differ 2019;26(9):1796–812.
[53] Wu Q, Sun L, Hu X, Wang X, Xu F, Chen B, et al. Suppressing the intestinal farnesoid X receptor/sphingomyelin phosphodiesterase 3 axis decreases atherosclerosis. J Clin Invest 2021;131(9).
[54] Qin Z, Dai L, Trillo-Tinoco J, Senkal C, Wang W, Reske T, et al. Targeting sphingosine kinase induces apoptosis and tumor regression for KSHV-associated primary effusion lymphoma. Mol Cancer Ther 2014;13(1):154–64.
[55] Cheng C, Wang T, Song Z, Peng L, Gao M, Hermine O, et al. Induction of autophagy and autophagy-dependent apoptosis in diffuse large B-cell lymphoma by a new antimalarial artemisinin derivative, SM1044. Cancer Med 2018;7(2):380–96.
[56] Brown EM, Ke X, Hitchcock D, Jeanfavre S, Avila-Pacheco J, Nakata T, et al. Bacteroides-Derived Sphingolipids Are Critical for Maintaining Intestinal Homeostasis and Symbiosis. Cell Host Microbe 2019;25(5).
[57] Zhang S, Huang P, Dai H, Li Q, Hu L, Peng J, et al. TIMELESS regulates sphingolipid metabolism and tumor cell growth through Sp1/ACER2/S1P axis in ER-positive breast cancer. Cell Death Dis 2020;11(10):892.
[58] Ries RJ, Zaccara S, Klein P, Olarerin-George A, Namkoong S, Pickering BF, et al. m(6)A enhances the phase separation potential of mRNA. Nature 2019;571 (7765):424–8.
[59] Tan B, Liu H, Zhang S, da Silva SR, Zhang L, Meng J, et al. Viral and cellular N(6)-methyladenosine and N(6),2'-O-dimethyladenosine epitranscriptomes in the KSHV life cycle. Nat Microbiol 2018;3(1):108–20.
[60] Zhong L, Liao D, Zhang M, Zeng C, Li X, Zhang R, et al. YTHDF2 suppresses cell proliferation and growth via destabilizing the EGFR mRNA in hepatocellular carcinoma. Cancer Lett 2019;442:252–61.
[61] Qiu L, Chen L, Yang X, Ye A, Jiang W, Sun W. S1P mediates human amniotic cells proliferation induced by a 50-Hz magnetic field exposure via ERK1/2 signaling pathway. J Cell Physiol 2019;234(6):7734–41.
[62] Ramdas B, Yuen LD, Palam LR, Patel R, Pasupuleti SK, Jideonwo V, et al. Inhibition of BTK and PI3Kdelta impairs the development of human JMML stem and progenitor cells. Mol Ther 2022;30(7):2505–21.
[63] Gaudio E, Tarantelli C, Kwee I, Barassi C, Bernasconi E, Rinaldi A, et al. Combination of the MEK inhibitor pimasertib with BTK or PI3K-delta inhibitors is active in preclinical models of aggressive lymphomas. Ann Oncol 2016;27(6):1123–8.
[64] Ma J, Zhao S, Qiao X, Knight T, Edwards H, Polin L, et al. Inhibition of Bcl-2 Synergistically Enhances the Antileukemic Activity of Midostaurin and Gilteritinib in Preclinical Models of FLT3-Mutated Acute Myeloid Leukemia. Clin Cancer Res 2019;25(22):6815–26.